



Review

Corrosion Barrier Coatings: Progress and Perspectives of the Chemical Route

George Kordas 

Self-Healing Structural Materials Laboratory, Peter the Great St. Petersburg Polytechnic University,
195251 St. Petersburg, Russia; gckordas@gmail.com

Abstract: Improved corrosion barrier coatings (CBCs) to protect metals will allow future metal structures to operate for extended periods, ensuring improved safety by reducing environmental pollution and maintenance costs. Many production methods and design of corrosion barrier coatings (CBCs) have been developed. This review focuses only on CBCs made with chemistry techniques. These CBCs can be passive and active with remarkable performance. Today, most of the work focuses on the discovery and application of “smart nanomaterials,” which, if incorporated into “passive CBCs,” will turn them into “active CBCs,” giving them the phenomenon of “self-healing” that extends their service life. Today, many efforts are focused on developing sensors to diagnose corrosion at an early stage and CBCs that self-diagnose the environment and respond on demand. In addition, recent technological developments are reviewed, and a comprehensive strategy is proposed for the faster development of new CBC materials.

Keywords: corrosion; barrier; coatings; self-healing; nanocontainers; CBC



Citation: Kordas, G. Corrosion Barrier Coatings: Progress and Perspectives of the Chemical Route. *Corros. Mater. Degrad.* **2022**, *3*, 376–413. <https://doi.org/10.3390/cmd3030023>

Academic Editors: Mikhail Zheludkevich, Viswanathan S. Saji and Kiryl Yasakau

Received: 19 April 2022

Accepted: 14 July 2022

Published: 19 July 2022

Publisher's Note: MDPI stays neutral with regard to jurisdictional claims in published maps and institutional affiliations.



Copyright: © 2022 by the author. Licensee MDPI, Basel, Switzerland. This article is an open access article distributed under the terms and conditions of the Creative Commons Attribution (CC BY) license (<https://creativecommons.org/licenses/by/4.0/>).

1. Introduction

Heavy metal compounds to protect metals from corrosion, such as Cr(VI) and Cr(III), exhibit toxicological properties, and their replacement with ecological corrosion barrier coatings (CBC) is of high technological and social importance. Furthermore, vapors and dust containing Cr (VI) inhaled by living organisms cause DNA modification in living cells, resulting in brain and lung cancer [1,2]. Assuming that approximately 2 g Cr(VI) is used per car to protect against corrosion, the automotive industry consumes at least 30 tons Cr(VI) per year at the European level. Many of these quantities are later released uncontrollably into the environment by waste disposal [3]. An environmental study in Denmark revealed that at least 2–4 tons of Cr(VI) per year are emitted into the water from surface treatment or wastewater from related industries, and 16–33 tons are released into the soil [4]. By extension, much more than 100 tons of Cr (VI) per year are still released in Europe [4]. In 2006, European legislation called “REACH” was developed, obliging companies managing hazardous chemicals not to consume more than 1 ton per year [5]. Consumption above this limit imposes a special authorization by the European Chemicals Agency (ECHA) valid for a set period [6]. As a result, companies have started to look for other eco-friendly protective coatings instead of chromium(VI) compounds. As realized by hexavalent chromium, innovative technologies must ensure competitive costs and high-efficiency anti-corrosion performance. The replacement of hexavalent chromium can be done with hexafluorozirconate (ZrF_6^{2-}) [7–13]. However, the absence of hexavalent chromium within the coating reduces self-healing properties [13]. The Alodine T 5900 RTU by Henkel and the Socosurf TCS by Socomore conversion coatings and surface treatments are based on trivalent chromium and are REACH compliant alternatives to Cr(VI) [14,15]. The production process of these products leads to the partial oxidation of the Cr^{3+} to Cr^{6+} with a percentage not exceeding 0.1 wt% that satisfies the REACH Directive [16–19]. Chromium chloride ($CrCl_3$) and chromic oxide (Cr_2O_3) have been shown to be genotoxic

in vitro, where chromosomal aberrations (CAs) were found in human lymphocytes [20,21]. The significant DNA migration caused by CrCl_3 was found in human lymphocytes [22]. The diet supplement chromium(III) tris(picolate) ($\text{Cr}(\text{pic})_3$) may cause CAs hprt mutations and single-strand breaks [23–25]. A study showed that workers' exposure to trivalent chromium could indicate detectable DNA damage in peripheral lymphocytes [20]. Cerium conversion coatings were produced on aluminum alloy 2024-T3 to offer corrosion resistance because they tend to form hydroxides at a pH of >10 , preventing cathodic reactions on corrosive surfaces. The cerium obtains the Ce^{4+} form. In an acidic environment, these oxides are dissolved, and the coatings do not provide any more protection [26]. Lately, Zirconium based CBC were developed [27], which meets the chromium replacement requirements and thus offers excellent potential for further applications. Many patents show the maturity of this technology [27–30], which the automotive industry has exploited since 2005 [27,31,32]. In addition, there are numerous references in the literature that summarize this emerging technology [31–36]. Zirconium-based conversion coatings (ZrCC) offer many advantages because they have low environmental impact in addition to being economical [37–39]. Recently, Zr and Ce combinations (ZrCeCC) have been studied, which have been shown to provide a synergistic effect in terms of barrier and self-healing for corrosion inhibition [26]. The conversion coatings are created from chemical procedures [40], atomic layer deposition (ALD) [41], and chemical vapor deposition (CVD) [42] methods on metal surfaces. The production of CBC will limit this review only to chemical techniques for space reasons.

Chromium(VI) replacement started with alkoxide-based sol-gel coatings on metals, but the disadvantages became apparent, and the idea was abandoned [43]. Then, ORMOSIL-type coatings were developed with impressive results [44]. Furthermore, the development and evaluation of inhibitors required extensive experimental and theoretical work [45,46]. The development and integration of nanocontainers loaded with inhibitors and their incorporation into polymeric CBC present a significant milestone in the field [47,48]. These integrated systems exhibit the self-healing phenomenon [49]. The self-healing phenomenon was discovered for the first time in polymers by Malinskii in 1969 [50]. Wool considered healing phenomena in polymers that restore deformation to the original state [51,52]. In 2001, White reported a polymeric material stored in nanocontainers that can autonomously heal cracks [53]. Today, investigators are focusing on finding even intelligent nanostructures that react to external stimulations, e.g., pH change exhibiting multifunctionality. This significant progress occurred via the close collaboration of scientists from materials science, chemical engineering, and corrosion science. The success of the new CBC technology imposes close collaboration of scientists with diverse talents collaborating closely with the paint industry and metal end users for the successful implementation of this technology. This paper looks back at this technology's developments and further sets milestones to achieve in science in this field. This publication will not deal with the substrate because this was the subject of another recent review [40]. The development of intelligent CBCs through chemical techniques is a multidimensional task that requires many individual stages, such as the development of corrosion-resistant coatings, the finding and evaluation of corrosion inhibitors suited for each metal surface, the development of nanocontainers efficient to protect the metallic surface, and finally the development of sensors that will automatically diagnose the condition of the coatings. Figure 1 shows the individual tasks to find ecological CBCs that exhibit the phenomenon of "self-healing".

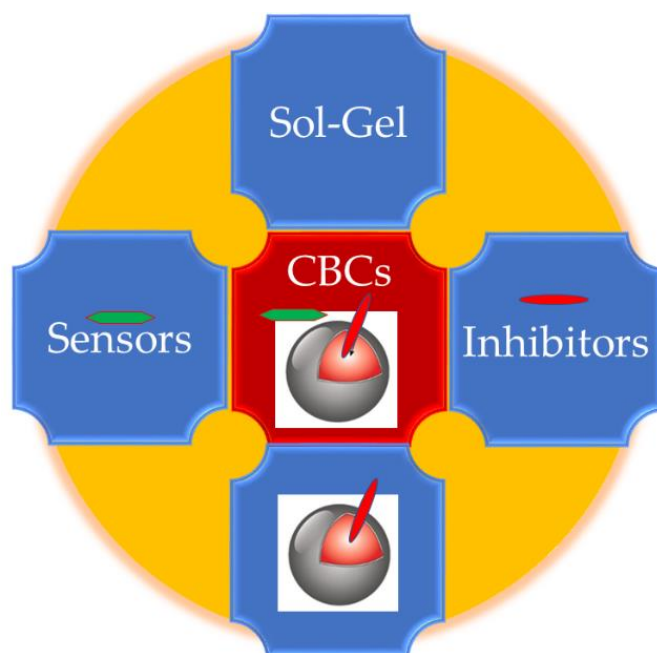


Figure 1. Schematic illustration of the steps taken to replace chromium (VI) CBC with ecofriendly CBC exhibiting the self-healing phenomenon.

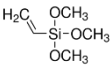
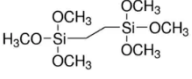
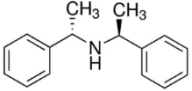
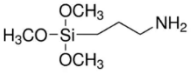
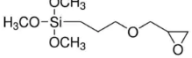
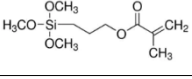
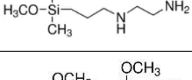
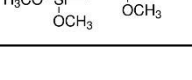
2. Sol-Gel Processing

The sol-gel method produces glass and ceramic materials at lower temperatures than the corresponding products molded by melting. This method uses alkoxides, water, catalyst, and solvent [54]. Depending on the relationship between alkoxide/water and the kind of catalyst [54,55], one can obtain a one-dimensional, two-dimensional, or three-dimensional network where one takes fibers, thin films, or bulk materials. Some years ago, scientists attempted to produce coatings on metals to protect against corrosion [43,56]. Using a multiple immersion technique in the sol solution followed by a densification process, they deposited on copper, nickel, iron, and aluminum metals protective ZrO_2 , SiO_2 , TiO_2 , and $B_2O_3-3SiO_2$ coatings. They were using the dip-coating method of metals in the sol solution, where they were first left to dry and next heat-treated slowly ($5\text{ }^\circ\text{C}/\text{min}$) up to the temperature of $500\text{ }^\circ\text{C}$. The effectiveness of the sol-gel coatings against corrosion in the early studies was examined with weight loss measurements by exposing them to salt solutions. These studies revealed that the protection offered by the coating depends on its thickness. The increased thickness led to cracks during their thermal densification treatment or the alternating temperature during operation [56]. From the above studies, inorganic oxide coatings can protect metal substrates but do not significantly replace chromium-based CBCs [43]. One needs to reduce the densification temperature to $200\text{ }^\circ\text{C}$ to avoid the metal's destruction and develop flexible coatings that will adapt their physical properties (e.g., anticorrosion protection, the thermal expansion coefficient of the coating) to the properties of the metal. To realize that requirement, one needs precursors consisting of two primary components, the one organic and the other inorganic, the one responsible for the flexibility of the CBC, and the other for the anticorrosion properties.

3. Silanes

Silanes are hybrid organic-inorganic compounds used to help alleviate the problem occurring in the traditional sol-gel technology. Table 1 gives some chemical formulas of silanes/bis-silanes used to start the discussion [57]. These CBCs based on these precursors have proven effective in recent years [44]. Their hybrid structure maximizes their effectiveness against corrosion and their properties for primary technological needs.

Table 1. The structures of some silanes/bis-silanes.

Material	Structure
Vinyl trimethoxy silane	
Bis-1,2-(trimethoxysilyl) ethane	
Bis-[trimethoxysilylpropyl]amine	
(3-Aminopropyl)trimethoxysilane	
3-Glycidyloxypropyl- trimethoxysilane	
3-(Trimethoxysilyl)propyl methacrylate	
3-(2-Aminoethylamino)-propyldimethoxymethylsilane	
1,2-Bis(trimethoxysilyl)ethane	

The concentration of silanes, the water amount, the pH of the solution, the temperature of the reaction, and the aging of the solution affect the reaction's kinetics, the extent of hydrolysis, and the concentration of bis-1,2-(trimethoxysilyl) ethane (BTSE) in the solution. The speed of hydrolysis increases with the amount of water, while the speed of condensation is a function of BTSE concentration [44,58]. CBCs have been produced with BTSE [59,60] using methanol solutions due to the low solubility of BTSE in water [61]. Methanol cannot be used in industrial processes due to its health dangers. This process leads to the formation of many monomers that living organisms can absorb. Thus, water-based chemistry was developed to alleviate the problem. The question arose whether both chemistries produce the same coatings. In an extensive study [58], the CBCs produced with and without methanol solutions were examined concerning the microstructure [62]. The aqueous chemistry yields more high molecular weight species, indicating that the aqueous solution BTSE is less reactive and newsworthy without health hazards. The resulting structures are similar in both cases. Another aspect of the silanes is their ability to be mixed with two or more substances, such as epoxy resins, polymers, and others. The procedure allows for economical upscaling. The silane CBC facilitates tiny pores allowing the diffusion of the electrolyte and the accumulation of corrosive species on the interface coating/substrate, resulting in corrosion. Researchers attempted to create a single layer with a larger thickness that was brittle, but the solution's stability during deposition was small [63]. It is worth noting that silanes are not electrochemically active substances in solution or solid-state and are not reduced or oxidized unless they have electrochemically active groups. Therefore, they act as barrier coatings. In summary, the silane coatings are hydrophobic and exhibit barrier properties. Their barrier properties prevent water, oxygen, and corrosive ions from reaching the metal substrate [64]. However, a silane film alone cannot effectively protect the metal from corrosion for a long time due to its small thickness, which quickly becomes saturated by the corrosive solution and thus ceases to act as a barrier [65]. This drawback has led to the search for complex systems such as metal/silane/organic coatings to reach greater efficiency and limit the migration of metal ions through the coating [66]. The resulting systems from these works resulted in protective

coatings that were more stable with exposure to corrosive environments. The silane acts as a barrier to improve the adhesion between the metal and the organic coating, as in the case of epoxy resins [67], polyamides [68], and the mixture of epoxy/polyamide [69]. One research paper showed resistance to corrosion of metal AA2024-T3 silane-coated bis-[3-(triethoxysilyl)propyl] tetrasulfide (BTESPT). A water silane/DI/methanol solution equal to 4/5.5/90.5 vol% was used to immerse the metal. Afterward, blowing air at 120 °C for 40 min dried the coating. The same metal was pretreated with the standardized commercial (VI)-based TURCO™ Accelagold used as a reference sample. Electrochemical studies were performed using a 0.1 N NaCl solution. The silane membrane protected the substrate better than the reference chromate pre-treatment offered. In addition, the adhesion of BTESPT to the metal was facilitated by sulfur in the silane molecule [70]. One study showed that the overlap of (3-Glycidyloxypropyl) trimethoxy silane (GPTMS)-tetraethyl orthosilicate (TEOS)-ammonium persulfate based on silanes showed good protective properties for steel [71]. Many researchers reported electrolytic polypyrrole (PPy) coatings being deposited on steel in the presence of oxalic acid with spectacular results for metals in the iron series [72–77]. Although it is not entirely clear in the literature, due to the interaction of metal and polymer through galvanic coupling and upward polarization of the substrate, PPy provides anticorrosion protection for steels [78–81]. Finally, we must point out the difference between bis-silanes and silanes. Silanes have one Si atom per molecule, while bis-silanes have two Si atoms per molecule associated with three OR groups and six OR groups. Bis-silanes and silanes produce six SiOHs and three SiOHs per molecule during hydrolysis, respectively. After condensing the SiOH groups, bis-silanes create a denser network than do silanes.

4. ORMOSIL

a. Precursors and Reactions

ORMOSILs are prepared as organically modified silicate solutions that react with organic groups derived from an epoxy resin and a hardener. A series of solutions is prepared using the above ingredients in different proportions to select a suitable final product with the most satisfactory properties.

b. Organically Modified Silane

The reported silica alcohols or “silanes” are in the form of $R'-Si(OR)$, where R' is an organic group reacting with an organic polymer. In contrast, group R is an alkoxy group capable of participating in hydrolysis and condensation reactions. For example, a silane that can be used has the trade name Z 6020, while in the literature, it is found as *N*-(2-aminoethyl)-3-(trimethyloxypyl) propylamine with a molecular weight of 222.

c. Epoxy Resin

Epoxy resins are compounds, which contain at least one epoxy ring ($-CHOCH_2$) as an essential component of their monomer, i.e., they consist of an organic root and an oxygen atom joined to two carbon atoms [82]. The ring mentioned above is very active and is responsible for the vast number of products resulting from its reaction with several hardening agents. There are three classes of epoxy resins that are cycloolephatic, where there are six-membered rings in the organic part. The epoxy oils contain inseparable fatty acids and glysidic resins, whereas the organic part is a combination of hydrogenic polybasic acids or poly-hydro phenols [82]. They belong to the category of thermosetting polymers, i.e., their original properties are altered irreversibly via heating above a specific temperature.

A basic resin used to create the ORMOSIL membranes can be the bisphenol A diglycidyl ether (DGEBA) condensed with epichlorohydrin. The result of condensation is the creation of an epoxy group at the end of each polymer. The trade name of the product is DGEBA η Bisphenol A or GY-257, and the name found in the literature is phenol 4,4'-(1-methylethylidene) bis-, or phenol 4,4' isopropylidenedi- and belongs to the third category of epoxy resins. The presence of the benzene ring in the DGEBA molecule con-

firmly that the material becomes more rigid and stiffer in a short time when applied in a suitable environment.

d. Hardener

As its name suggests, the hardener is a substance that hardens some other compounds. For example, one can use diethylenetriamine as a hardener with triethylenetetramine (TETA) or HM 943.

e. Solvents

The solvents used to prepare this solution are a mixture of pure ethyl alcohol and acetone. The presence of both solvents ensures the proper dissolution of the precursors at the molecular level and ensures the necessary homogeneity. Therefore, the purity of solvents should be 99.9%.

f. Preparation of ORMOSIL

Figure 2 shows the mixing procedures of the components and their corresponding concentrations schematically.

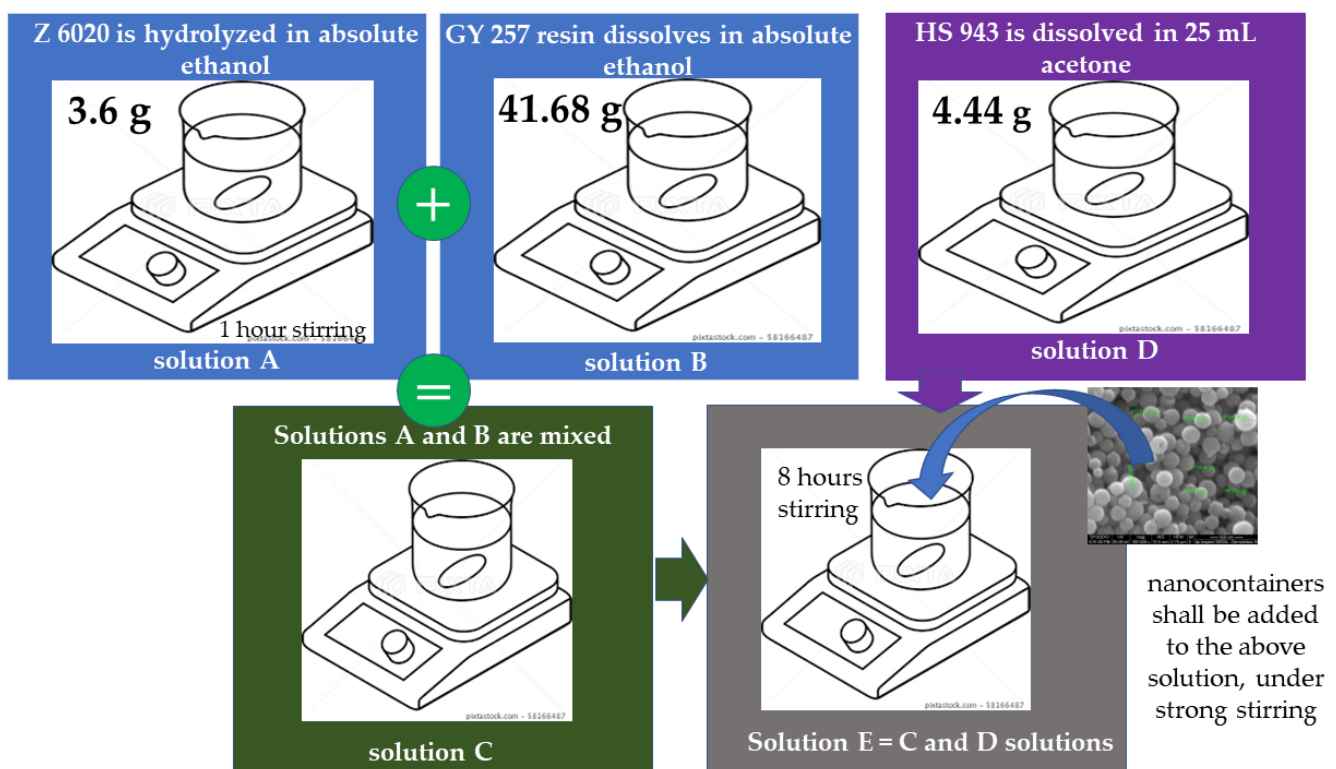


Figure 2. An example of CBC synthesis using the ORMOSIL method. Z 6020: N-(2-aminoethyl)-3-(trimethoxypropyl) propylamine, GY-257: phenol 4,4'-(1-methylethylidene) bis-, HM 943: triethylenetetramine.

Figures 3–5 show the individual reactions.

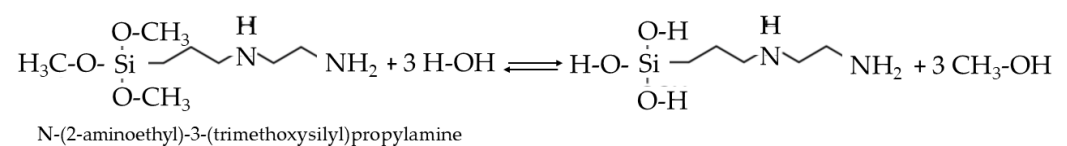


Figure 3. Hydrolysis of ORMOSIL.

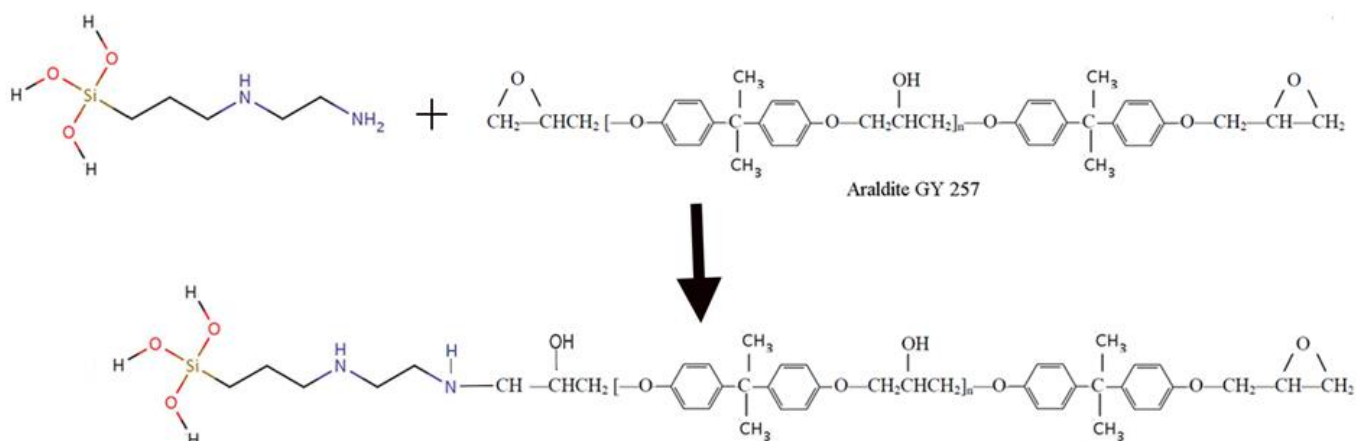


Figure 4. Epoxy group reaction with primary amine.

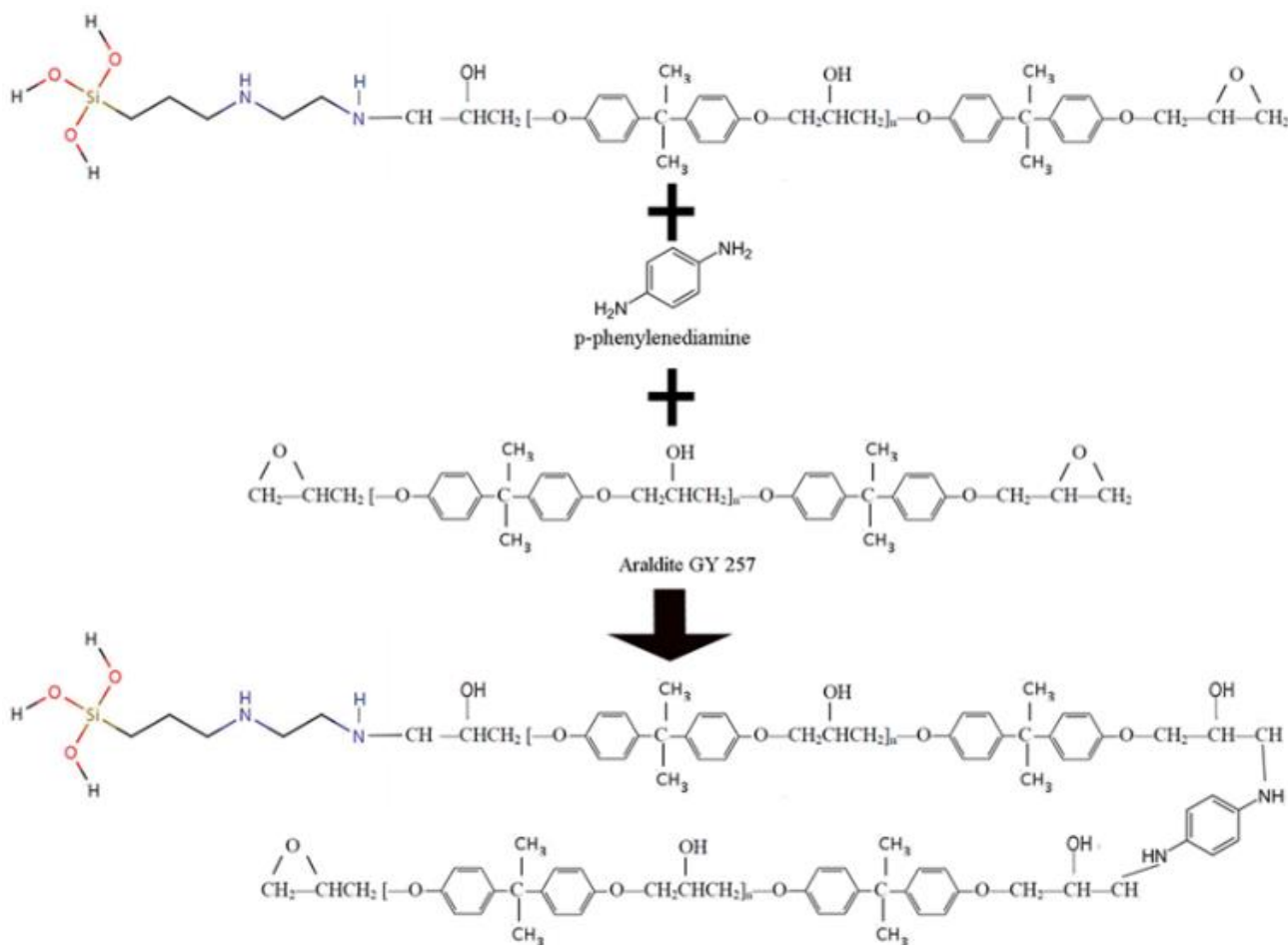


Figure 5. Synthesis of epoxy resin—ORMOSIL.

The surface-cleaned metals are immersed in the finished solution with or without the nano-containers six times at, e.g., a 32 cm/min speed and remain in the diathesis for one minute. Then, the coatings are heated at 70 °C for four days. Figure 6 shows the reactions occurring in this process.

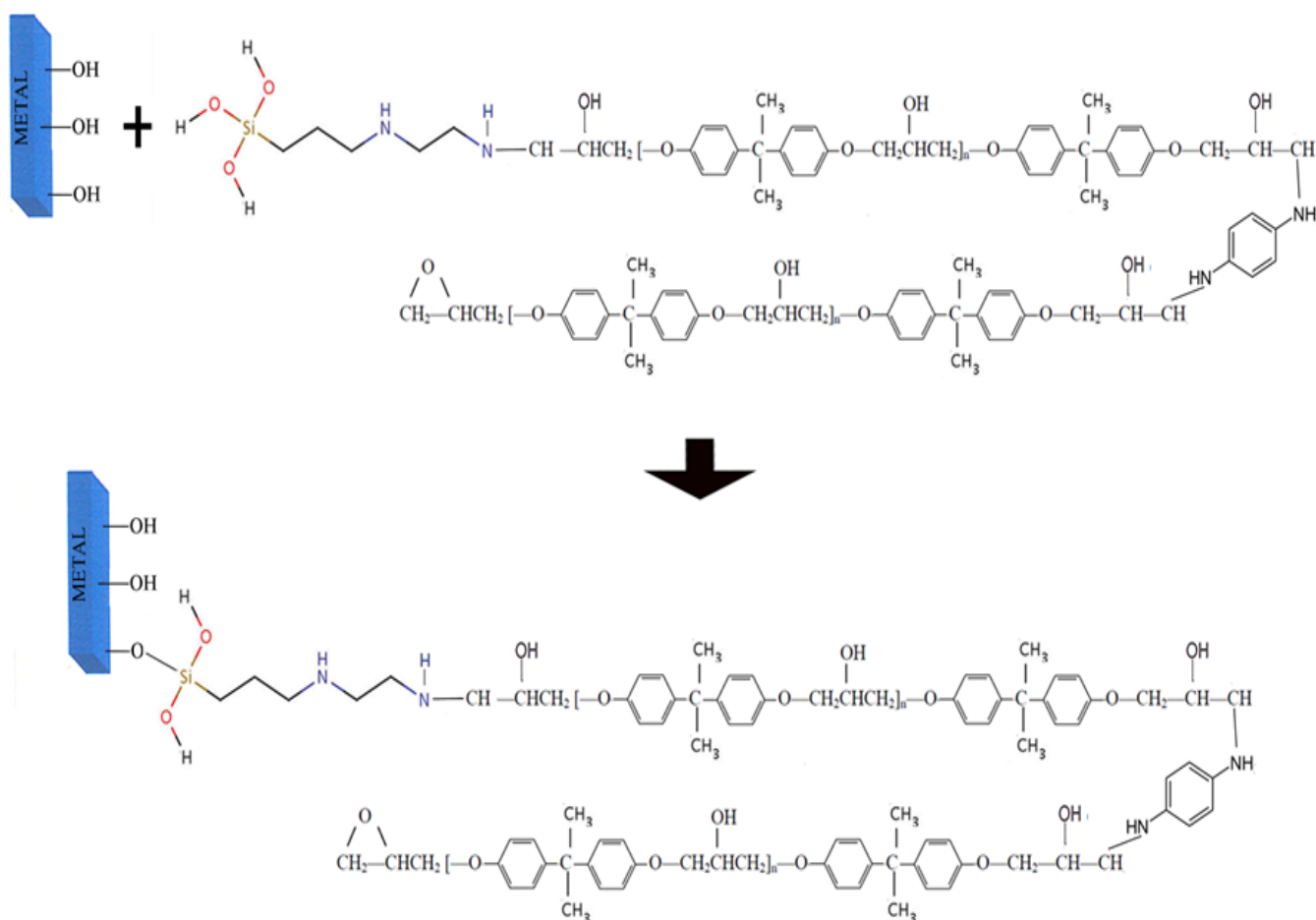


Figure 6. Attachment of a hybrid coating to the surface of the metal.

Figure 7 shows the EIS diagram of the bare sample (Sample 1), ORMOSIL coated (Sample 2), ORMOSIL coated + CeO₂ (Empty) (Sample 3), and ORMOSIL coated + CeO₂(5-ATDT) (Sample 4) [40,83]. The measurement showed that the ORMOSIL coating offered protection to the HDG metal. The metal had an $R_p = 1.73 E^{+03} \text{ Ohm cm}^2$, while the metal protected with ORMOSIL had a protected metal with ORMOSIL $R_p = 1.55 E^{+04} \text{ Ohm cm}^2$. When CeO₂ (empty) nano-containers were added to ORMOSIL, $R_p = 9.32 E^{+04} \text{ Ohm cm}^2$ and increased to $R_p = 3.05 E^{+05} \text{ Ohm cm}^2$ when the nanocontainers were loaded with 5-ATDT corrosion inhibitor [40,84]. The effect of coating the metal with ORMOSIL + CeO₂ (5-ATDT) was the increase of R_p in this sample by 1033.60, 109.21, and 7.76 from the steel samples HDG, HDG-ORMOSIL, and HDG-ORMOSIL + CeO₂ (EMPTY), respectively. This sample exhibited the “self-healing” phenomenon [84].

The thickness, structure, and corrosion resistance were investigated concerning the type and concentration of the solvent for which they were produced by mixing 11.2 mL of tetraethyl orthosilicate (TEOS), 15.2 mL vinyltrimethoxysilane (VTMOS), and 4.0 mL 3-(trimethoxysilyl) propyl methacrylate (MEMO) with 19.6 mL 0.05 M HNO₃ [85]. Solvent concentrations ranged between 28.5 and 66.5 vol.% and were non-polar solvents (hexane, heptane), aprotic polar solvents (acetone, MEK), primary alcohols (methanol, ethanol, isopropanol, 2-methoxy ethanol, 2-ethoxyethanol, 2-methyl-1-butanol, 3-methyl-1-butanol), secondary alcohols (1-methoxy-2-propanol), and tertiary alcohols (t-amyl alcohol). In summary, corrosion resistance depends on the type and concentration of the solvent. They found that high solvent concentrations lead to coatings with enhanced resistance to corrosion using aprotic solvents. Minor alcohols yield enhanced corrosion protection at low diluent concentrations. High concentrations of large alcohol diluents degrade the corrosion resistance of the ORMOSIL membrane. This work offered a benchmark

between structure–corrosion–the type of solvent–the solvent quantity that is useful for a researcher [85]. ORMOSILS were prepared with 3-glycidoxypropyltrimethoxysilane (GLYMO)–TEOS through the sol–gel method using nitric acid for the complexation of GLYMO and TEOS. As a result, a solid state of ^1H – ^{13}C and ^1H – ^{29}Si CP/MAS NMR led to the organic content determining the microstructure, and thus the anti-corrosion capacity of ORMOSIL. Moreover, the microstructure of ORMOSIL and the method of deposition affects the structure and, consequently, the anti-corrosive performance characteristics [86].

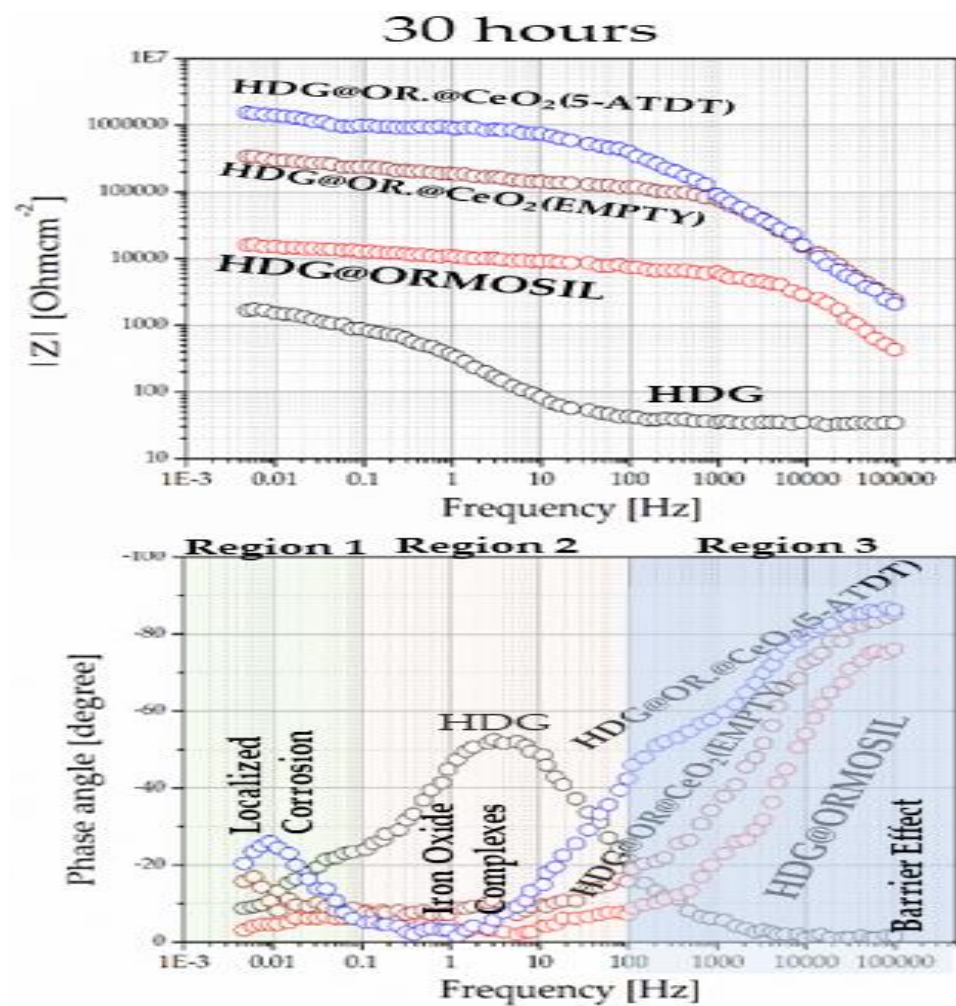


Figure 7. FRA of the samples HDG, HDG@ORMOSIL, HDG@ORMOSIL@CeO₂ (EMPTY), and HDG@ORMOSIL@CeO₂ (5-ATDT) exposed to a 0.5 M NaCl corrosive environment at ambient temperature [84].

5. Water-Based Commercial Sol-Gel CBCs

Chemetall GmbH developed the product OXSILAN AL-0500 based on silane for 2024, 2219, 5083, and 7075 aluminum [87]. These panels underwent multiple coatings with a solvent-free epoxy primer type MIL-DTL-53022, an epoxy primer without water type mil-DTL-53030, and a coating of polyurethane lymphatic type MIL-PRF-85285. As a result, the effects of accelerated corrosion were acceptable in some cases [87].

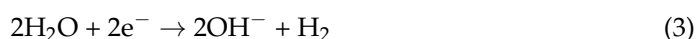
Boeing developed an anticorrosive sol–gel CBC using Zr(IV) n-isopropoxide and 3-glygodopropyltrimmethoxysilane (GLYMO) as organosilane compounds. Acetic acid was the catalyst. The anticorrosive sol–gel CBC exhibited excellent adhesion to the metal. Accordingly, the CBC with the trade name “Boegel” provides exceptional barrier properties to the metal without needing a further anticorrosive layer [88].

6. Inhibitors

6.1. Inorganic

Parallel to the advancement in the chemistry of coatings, considerable progress was made to add functionality to the CBCs by incorporating corrosion inhibitors, which can be organic, inorganic, or a combination of both.

The protection of the metal substrates from corrosion with the aqueous cation Ce(III) is done by creating an oxide–hydroxide membrane at the cathodic spot of the metal. The cathode reaction mechanism depends on the pH. In a neutral and basic environment [89], the reactions that take place in the presence of oxygen are:



In contrast, in an acidic environment, one obtains the following reactions:



The simplified reaction describes the anodic metal sites:



Reactions lead to dissolved metal cations whose stability depends on the pH of the solutions and the presence of, e.g., chlorine ions. For example, when the cerium is found on a metal surface, e.g., aluminum, and the pH is increased to 8, the following reaction takes place [90–92]:



At the same time, oxidation occurs in the solution:



The oxidation of Ce(III) in Ce(IV) occurs near the surface of the metal if the pH is above 8.7 [93].

The X-ray absorption method (XANES) was used to investigate cerium-containing films on aluminum and 5052 alloys [90]. The research was based on the analysis of the Ce L3 (6548 eV) and Ce L1 (6548 eV) absorption edges, which are characterized as 3 and 4 valent cerium. When aluminum was immersed for five days in a bath with Ce³⁺ ions at neutral pH, it was found to be Ce³⁺. After seven days of submergence in the same solution, Ce³⁺ oxidized to Ce⁴⁺. The valence state of the cerium depends on the time of exposure to the solution. In a zinc and iron metal, the deposition of cerium oxide above the substrate presupposes the formation of the hydroxide of the metal itself, which is rapidly removed and has a lower deposition of the compounds of cerium [94].

The addition of compounds such as Ce(NO₃)₆H₂O and CeO₂ fine powder was also evaluated in the silane chemistry [95,96]. These enhancers, as one calls them in silane sol–gel chemistry, significantly improve the barrier property of sol–gel coatings combined with the anticorrosion properties of cerium ions [97–105]. The anticorrosion action of the cerium ions occurs via the passivation of the imperfections or cracks. In addition, the cerium ions act as cathode-like corrosion inhibitors by the precipitation of insoluble cerium hydroxide in regions of high pH [106,107]. The anticorrosion action of the cerium compounds occurs via the cerium III and IV reactions with the hydroxyl ions to form hydroxides in cathodic regions and act as a barrier of oxygen [103,108]. The literature has many references to the structure of cerium in coatings, reduction of porosity in coatings via cerium incorporation, reactions of cerium depending on the chemical environment,

etc. Corrosion of the hybrid sol–gel coating in the X13VD martensitic stainless steel was investigated as a function of cerium concentration [96]. EIS showed that the coating's best cerium concentration was 0.01 M. When the concentration passed this amount, then the barrier effect of the sol–gel coating was reduced. The increase in the cerium content of this limit increased the hydrophobic character of the coating. Concentrations of cerium above 0.01 M led to the modifications of the sol–gel network, thus reducing the anticorrosion abilities of the material.

Here, further discussion is not necessary. The reader can refer to the references regarding the beneficial effects of cerium on CBCs [109,110].

6.2. Organic

Corrosion control of metal structures to prevent metal dissolution in corrosive environments can be done using organic inhibitors. In corrosive solutions, heteroatomic (O, S, N, and P) and electrons in the coupled form function as outstanding corrosion inhibitors for metals. Organic inhibitors are usually incorporated into CBCs. The literature has extensively analyzed which inhibitors are suitable for which metals. The protective effects of 3-mercaptopropyl-5-amino-1H-1,2,4-triazole (A), 3-mercaptopropyl-5-amino-1H-1,2,4-triazole (B) and 3-mercaptopropyl(3-methyl butyl)-5-amino-1H-1,2,4-triazole (C) were studied on brass against corrosion using electrochemical methods [111]. When inhibitor concentrations exceed 0.10 mM, the protection degree is greater than 99%. The protection is attributed to the formation of the molecules of the inhibitors with zinc and copper. The effectiveness is explained by the assistance of quantum mechanical calculations where the HOMO and LUMO states were calculated. The B3LYP/6-311 DFT method with the G(d, p) basis set calculated HOMO, LUMO, ionization potential, electronegativity, absolute hardness, and softness in eV [111]. The difference between HOMO and LUMO gives the HLG gap calculated for A, B, and C equal to 5.75, 5.77, and 5.73 eV, respectively. The smaller the HLG gap is, the higher the reactivity of the inhibitor to bind to the metal, giving a stronger inhibition effect [112]. The experimental and theoretical calculations are in excellent agreement.

Linear sweep voltammetry studied the inhibition of 2-mercaptobenzothiazole (MBT) on copper in ethanol solutions. The presence of MBT shows one anodic process correlated with the oxidation of MBT, which leads to the formation of a film on the electrode. Surface-enhanced Raman spectroscopy (SERS) demonstrated oxidation of MBT forming polymeric complexes with copper and the ionized thiol form [113].

The inhibition abilities of 2-(2-aminophenyl)-N phenylhydrazinecarbothioamide (AP4PT), N,2-diphenylhydrazinecarbothioamide (D4PT), and 2-(2-hydroxyphenyl)-N-phenyl hydrazinecarbothioamide (HP4PT) were investigated for mild steel in H₂SO₄ experimentally as well as by quantum mechanical methods. According to gravimetric and gasometric experiments, the inhibition efficiency follows the order: AP4PT > HP4PT > D4PT. Furthermore, the quantum chemical parameters agree with the experiment-derived inhibition efficiency [114].

The corrosion protection mechanism of 2-mercaptobenzothiazole (MBT) in cerium chloride (CeCl₃) for the treatment of AA 2024-T3 was investigated to determine any synergistic effect between the two inhibitors. Several methods were employed, including image-assisted electrochemical noise, the split-cell technique, potentiodynamic polarization, electrochemical impedance spectroscopy (EIS), and scanning electron microscopy (SEM). As a result, 2-MBT was shown to protect AA 2024-T3 via the protective layer on its surface from corrosion in a 3.5% NaCl solution. Moreover, there was no synergy between 2-MBT and the Ce³⁺. Then, in the test period, 2-MBT offered better corrosion protection to AA 2024-T3 than CeCl₃ and 2-MBT+ CeCl₃ [115].

Salicylaldehyde, 8-hydroxyquinoline, and quinaldic acid were evaluated as inhibiting organic compounds on the corrosion of 2024 aluminum alloy in 0.05 M sodium chloride solution. A plethora of techniques were employed, including electrochemical impedance spectroscopy (EIS), scanning electron microscopy coupled with energy dispersive spectroscopy (SEM/EDS), X-ray photoelectron spectroscopy (XPS), and atomic force microscopy

coupled with scanning Kelvin probe (SKPFM). The conclusions are that the quinaldic acid, salicylaldehyde, and 8-hydroxyquinoline offer anticorrosion protection for AA2024 by developing a thin organic layer of insoluble complexes on the surface of the alloy [116].

There is intense activity to find environmentally friendly corrosion inhibitors. One such case is the two food spices such as 2,5-dihydroxy-1,4-dithiane (DDD) and 2,5-dimethyl-[1.4] dithiane-2,5-diol (DTDD), which do not cause pollution of the ecosystem [117]. DDD and DTDD eliminate oxidation products in the interface, while 0.5 M H_2SO_4 is used to combat corrosion products. Electrochemical measurements have shown that DDD and DTDD are cathode-biased Cu corrosion inhibitors in the medium H_2SO_4 . Furthermore, DDD was shown to perform better than DTDD. DFT calculations with a 6-311 G++(d,p) basis set determined the energy gap ($\Delta E = E_{\text{LUMO}} - E_{\text{HOMO}}$). As previously said, the ΔE determines the anti-corrosion performance of the DDD and DTDD corrosion inhibitor, which was 1.90 eV and 4.46 eV, respectively, supporting the EIS results. In addition, molecular dynamics (MD) simulations were performed on the adsorption of DDD and DTDD on the copper surface, which, together with the copper surface XPS measurements, have shown that adsorption is chemical with a mechanism depicted in Figure 8. However, there are misgivings about the viability of this high-cost study of DDD and DTDD. Nevertheless, the idea points the way to finding corrosion inhibitors from cheap natural products to develop a complete ecological anti-corrosion system.

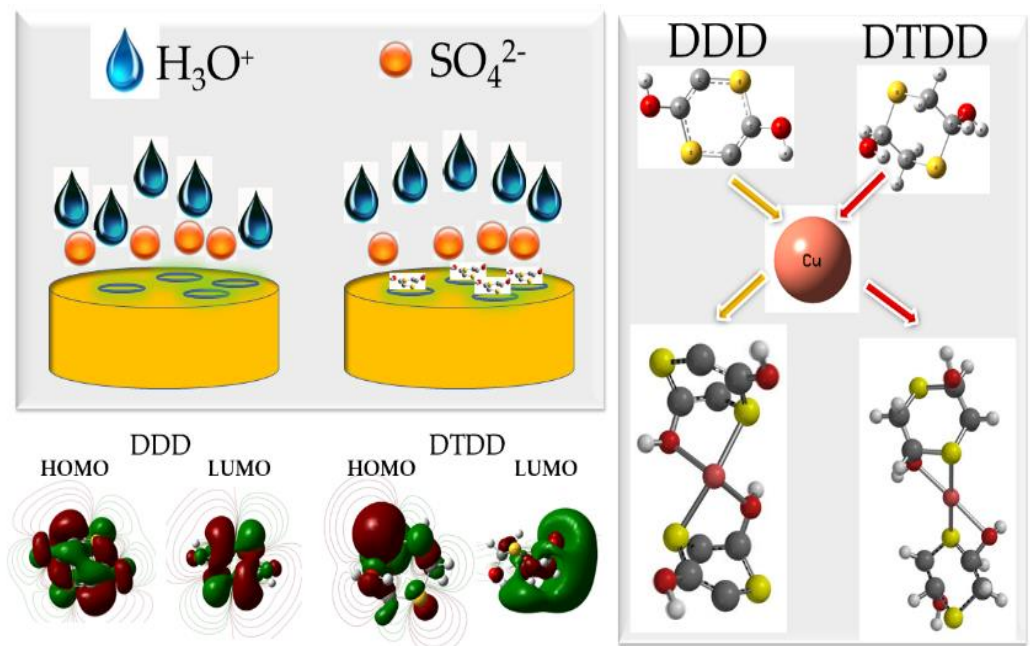


Figure 8. Absorption of DDD and DTDD mechanism onto copper.

The same group conducted research using *Passiflora edulia* Sims leaf extract (PESLE) using copper as a substrate exposed to 0.5 M H_2SO_4 , which functioned in ecological corrosion inhibition [118]. This was established after electrochemical and XPS studies. Quantum mechanics studies also supported the experiments.

7. Split Cell Technique

The split cell technique provides evidence of the corrosion inhibition mechanism of organic or inorganic inhibitors. The setup for this device (Figure 9) consists of two compartments connected via a porous membrane that allows electrons to pass. One immerses equal size specimens in the two compartments, and at this moment, the current density is near $0 \mu\text{Acm}^{-2}$. As shown in the above schematic, a zero resistance ammeter (ZRA) connects the AA 2024 T3 specimens (electrodes). When 15 min pass, nitrogen gas is merged in one of the compartments, and this specimen turns into a plain anode

as oxygen is depleted, leading to a reduction reaction. In the other compartment, air flows, allowing the other electrode to become an oxygen-available cathode. The current measured at this stage is generally of the order of $0.6 \mu\text{Acm}^{-2}$. One can add that 2-MBT in the anodic compartment induces a rapid current density drop and a potential increase, and in the cathodic compartment, one observes a slight current decrease and increased potential. With the addition of benzotriazole (BZT) into the two compartments in another experiment, one observes that current and potential values are unaffected. Here, 2-MBT decreases the anodic and cathodic reaction rates, preventing corrosion initiation [119]. The method accommodates equivalent circuits and extensive mathematics described in the literature [120]. The method is suitable for finding appropriate corrosion inhibition in an explicit metal substrate and is presented for future use by others.

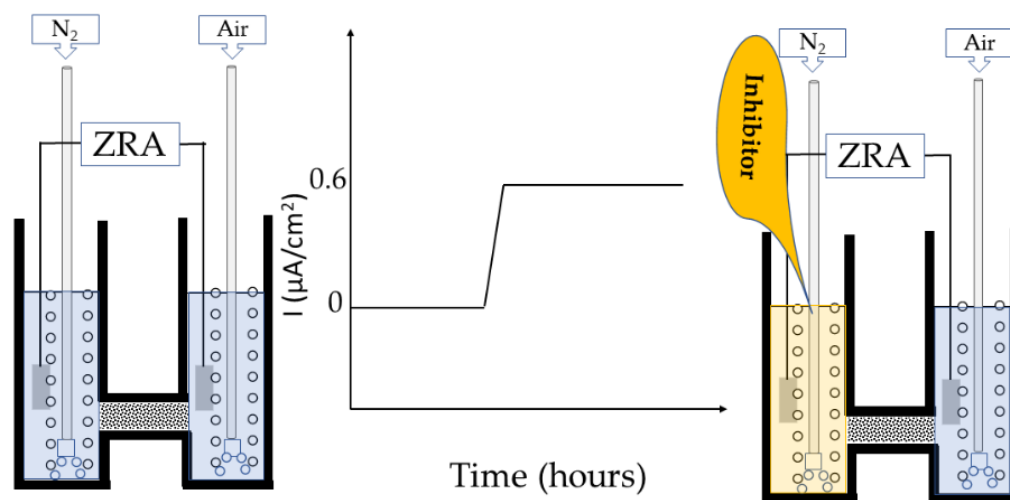


Figure 9. Split-cell electrochemical techniques.

8. Electrochemical Noise (EN) Method

Recent literature described the electrochemical noise (EN) method very extensively [120]. Figure 10A briefly sketches this method. Two equal electrodes are immersed in an electrolyte (3.5% NaCl) connected to a zero resistance ampere (ZRA) meter. The potentials of each electrode concerning a calomel electrode are recorded using an analog to digital converter. This device allows the corrosion phenomena to occur without electrical disturbance. This setup gives information about the anti-corrosion performance of corrosion inhibitors dissolved in the conductive electrolyte. Figure 10B gives the equivalent circuit of this device and the mathematical equations necessary for the analysis of the measurements [120]. The device has been experimentally validated and offers significant results in the performance of corrosion inhibitors. Initially, segments are exported to the original potential and current datasets. At the first point of the section, one produces the square root of the variance of the potential, $\sigma(V(t))$, divided by the variance of the current, $\sigma(I(t))$ (Figure 10B). Thus, one obtains the evolution of the values of the noise resistance. Figure 10 shows a standard measurement for a metal AA 2024-T3 without and with 0.15 mmol $\text{Ce}(\text{NO}_3)_3$. From a series of measurements involving $\text{Ce}(\text{NO}_3)_3$, $\text{Co}(\text{NO}_3)_3$, and $\text{Mn}(\text{NO}_3)_3$, $\text{Ce}(\text{NO}_3)_3$ offers the best anticorrosion performance [121]. The concentration of the inhibitor plays an essential role in the protection provided by these compounds. This method allows for recording the actual behavior of corrosion phenomena.

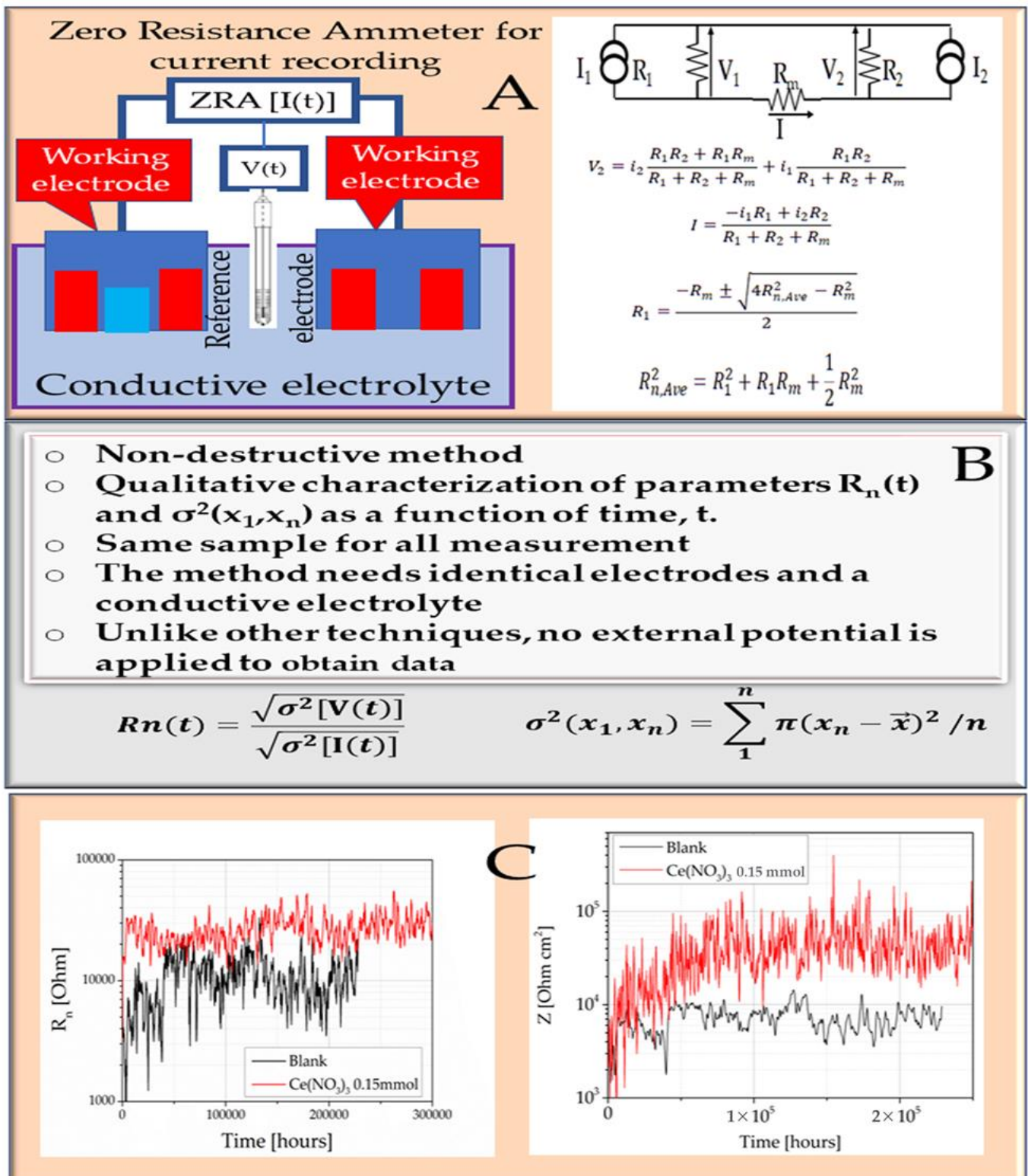


Figure 10. (A) Presentation of the electrochemical noise system, (B) $R_n(t)$ and $\sigma_n^2(x_1, x_n)$ equations, and (C) an example of an EN measurement involving an AA 2024-T3 in a 3.5% NaCl electrolyte with and without 0.15 mmol $Ce(NO_3)_3$.

9. Scanning Vibrating Electrode Technique (SVET)

The SVET technique maps the local current density on electrochemically active samples, such as a corroded metal within an electrolyte. Such an instrument consists of a

probe that measures the potential during vibration. The result is an AC dynamic measurement converted to DC potential with a lock-in amplifier that measures the DC current as a function of the x–y position of the probe. The SVET technique requires precise probe vibration through an accurate piezo vibrator. Figure 11 schematically describes such an SVET device. Figure 11 also shows a typical SVET measurement of metal coated with ORMOSIL doped with CeMo(MBT). The I_{anodic} and I_{cathodic} currents become equal to the noise values for longer period of times. Thus, one can suggest that self-healing occurs in the samples (Figure 11).

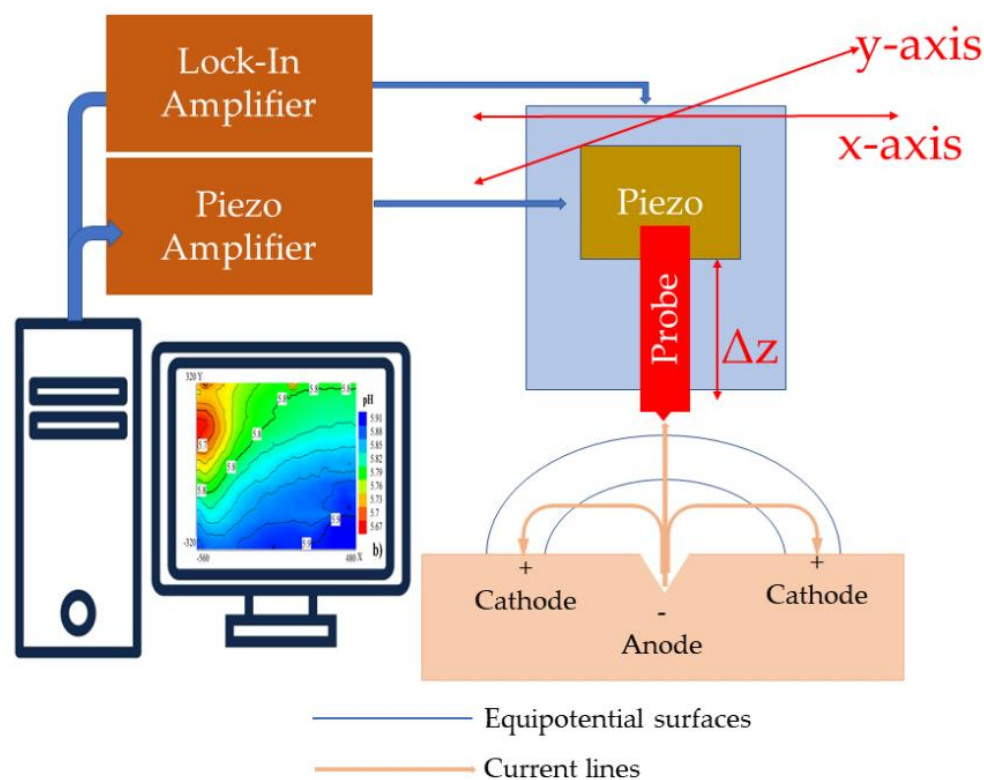
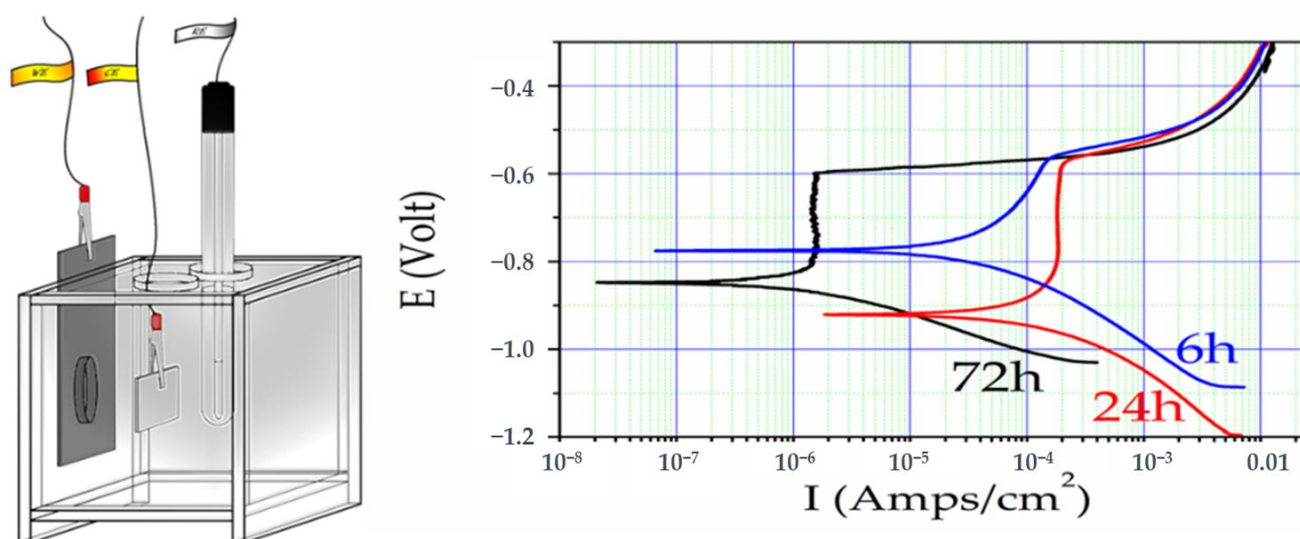


Figure 11. SVET set up showing a typical measurement across the x–y axis.

10. Organic Inhibitors in Nanocontainers

8-Hydroxyquinoline (8-HQ) acts as an inhibitor by preventing active sites of the metal surface [122]. In the above discussion, the inhibition action of cerium oxide has been discussed, forming a layer of pure cerium oxide on the metal surface [123]. In one publication, 110-nm ceria nanocontainers were reported to be loaded with 8-HQ [124]. This 8-HQ–CeO₂ complex is a system of organic and inorganic corrosion inhibitors involving nanocontainers. Figure 12 shows the polarization curves of the complex corrosion inhibitor after 6 (a), 24 (b), and 72 (c) hours of exposure to 0.5 M NaCl with the device depicted in the same picture. The included table gives R_p , I_o , and E_o acquired at 72 h of exposure. The polarization resistance (R_p) and corrosion current (I_o) show that protection of the aluminum panel is present after 72 h. The reduction of the anodic current after 72 h is due to the release of the inhibitor from the nanocontainers. These results show the release of the inhibitor from the nanocontainer, offering protection to the metal [124]. Figure 12 shows polarization curves (right) for bare AA2024 aluminum panels gained in the device (left) at 6, 24, and 72 h in 0.5 M NaCl in the presence of 8-HQ-loaded CeO₂ nanocontainers. After fitting the polarization curves, the R_p , I_o , and E_o values were gained.



Time (h)	R_p (Ωcm^2)	I_p (Acm^2)	E_p (mV)
6	9.28×10^2	2.81×10^{-5}	-774.50
24	2.87×10^2	9.08×10^{-5}	-920.03
72	1.76×10^4	1.40×10^{-6}	-847.04

Figure 12. Polarization curves of the 8-HQ-loaded CeO_2 nanocontainers as a function of the time in a salt solution obtained in the Plexiglas setup and results of fitting the polarization curves: the R_p , I_p , I_o , and E_p .

This result shows that cerium and 8-HQ act together as inhibitors that prevent corrosion of the metal.

11. Nanotechnology

After the first production of CBCs by the sol-gel method, their further progress turned to developing a generally applicable multifunctional corrosion coating technology based on nanoparticles or nanocontainers as functional design elements. The new nanotechnology not only had to replace the used corrosion protection systems based on toxic and environmentally hazardous compounds of heavy metals such as chromates but at the same time add third functions such as abrasion resistance, low surface tension, antifouling properties, antibacterial properties, self-healing of the anticorrosion properties of CBCs, anti-icing technology, etc. In addition, the nanoparticulate or nanocontainers must release controlled corrosion inhibitors to achieve active corrosion and self-healing protection of CBCs. In recent years, revolutionary nanotechnology has been developed that allows for the simultaneous establishment of active and passive protection against corrosion without using toxic compounds or heavy metals. The development of such technology is a complex process that is shown condensed in Figure 13, consisting of three main stages: the development of materials, the examination of their properties, and other supporting actions, including applying technology to demonstrators.

Cooperation with the industry is essential for the targeted development of multifunctional materials necessary to users. The understanding of phenomena requires a modeling approach to reveal the self-healing mechanism. This new nanotechnology-based approach must include pilot-scale production, industrial processing, and application technology.

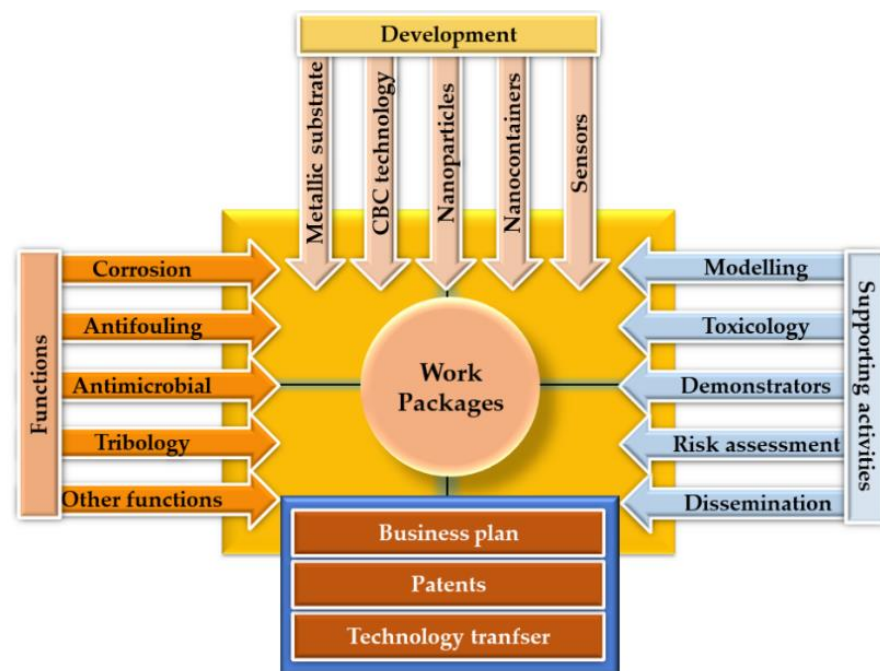


Figure 13. The basic structure of CBC development: from lab to industry.

11.1. Silanes and Nanoparticles

The addition of nanoparticles to the silane coating benefits the protection of metals from corrosion. A positive effect has been recognized for commercial and newly developed nanoparticles such as cerium dioxide, titanium oxide, cerium molybdate, aluminum hydroxide oxide, aluminum oxide, zirconium dioxide, strontium aluminum polyphosphate (SAPP), and silicon carbide [125–130]. These inhibiting materials have been incorporated into hybrid inorganic–organic hybrid sol–gel matrices to improve their behavior in corrosion protection. Especially, amorphous nanoparticles such as CeO_2 have shown improved performance against corrosion via pore-clogging, and by filling gaps and imperfections of the coatings [131–134]. Their presence in the coating leads to avoidance of crack formation, yielding higher mechanical durability and anticorrosion protection [109,135]. CeO_2 is very stable in alkaline pH. One study showed that the addition of CeO_2 in water-soluble silane film bis-1,2-triethoxysilolaethane (BTSE) exhibited excellent adhesion to the substrate and excellent anticorrosion properties in Al alloys [133], comparable to those of treatment with Cr(VI) [133,136]. The introduction of TiC, TiN, and TiC/SiC/Si₃N₄ (Ti–Si–C–N) improves the hardness of the coatings [137]. A study examined the size (nano- CeO_2 and micro- CeO_2 powders) and the concentration of particles embedded in various hybrid sol–gel coating systems to protect against corrosion of aluminum alloy AA2024. In the case of micro- CeO_2 , the coatings are vulnerable to corrosion. For the same level of doping as nano- CeO_2 , better corrosion protection is observed. At the same time, high loads with inhibitors harm corrosion protection [138].

A theoretical model simulated self-healing processes in coatings by combining Nernst equations with Fick’s diffusion law and other necessary equations [139]. The results of these calculations were confirmed by many experiments that rinses the inhibitor from a damaged coating containing cerium nanoparticles that released cerium to scratched metal, inducing corrosion. The model was used to describe the self-healing processes of the coatings as observed by the SVET technique [139]. For the proposed coating, the scale and time scale of the inhibitor release were calculated computationally. The permeability of the coating plays a significant role in releasing the cerium from the nanoparticles. These results suggest that the deviation of the values for such parameters from the nominal ones has a critical effect on the release rate of the inhibitors and, therefore, on the active protection against

corrosion. The calculations predicted the optimal inhibitor concentration and the stability of the coating concerning these parameters [140].

The effect of adding carbon nanotubes (CNTs) on the corrosion resistance of a tetra-sulfide bis(triethoxysylpropyl)propyl (BTESPT) film to a steel substrate was studied in one procedure. The coating was compact, with significant improvement in its anticorrosion capabilities [141].

11.2. CBCs with Nanocontainers

Protective coatings on metals against corrosion are divided into passive and active (Figure 14). Passive coatings provide a barrier to the corrosive environment until they are destroyed, e.g., scratched. When these coatings contain inhibitor-loaded nanocontainers, they turn into active ones. In the analogous case of damage, corrosion inhibitors are released from the nanocontainers and repair the damaged area of the coating [40]. The legitimate question is why one enters the process of incorporating corrosion inhibitors into nanocontainers. This is answered by the unwanted rinsing of the inhibitors from the coatings and deactivation of the inhibitor due to the complexation with the backbone of the coating that disables them [40]. Corrosion inhibitors incorporated into CBCs also negatively affect their properties [2,142]. The type of destruction depends on the loading CBC matrix with inhibitors. The solution to these problems involves a “smart” release of inhibitors achieved by encapsulation in nanocontainers, allowing them to be active on demand. In recent years, many nanostructures of different shapes, sizes, and compositions have been developed with different levels of effectiveness and with diverse methods of production. The corrosion inhibitors are released from the nanocontainers after changes in the pH, internal or external changes in the temperature, or the nanocontainers’ destruction. The pH change can be attributed to corrosion, i.e., the pH decreases (micro-anodes) in spots due to the dissolution of metals and hydrolysis reactions, while areas are increased (micro-cathode) due to oxygen reduction by the formation of hydroxide ions.

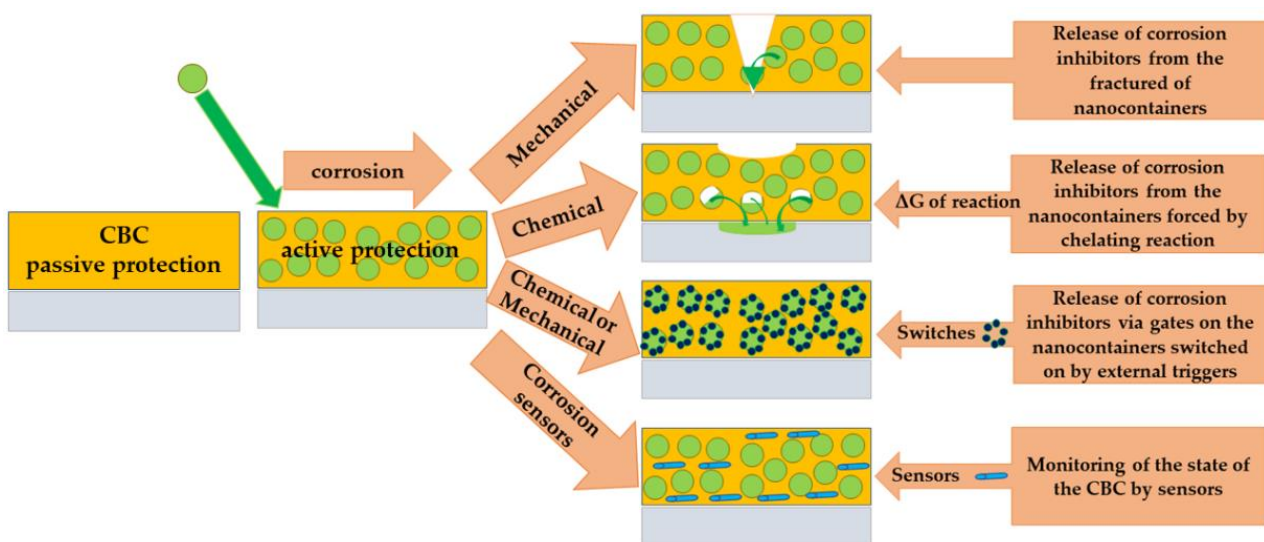


Figure 14. Milestones for the successful implementation of the technology.

Another parameter for selecting the nanocontainers is their compatibility with the coating chemicals and their homogenous dispersion in the CBCs. The material from the nanocontainer shell must be irresistible from any influence of coating production.

It is recommended to test the nanocontainers’ dispersion in the CBC any time after sample production [143], as shown in Figure 15. In some cases, its surface modification is necessary to ensure repulsion between the nanocontainers during mixing with the coating resins to achieve homogeneous distribution in the paint.

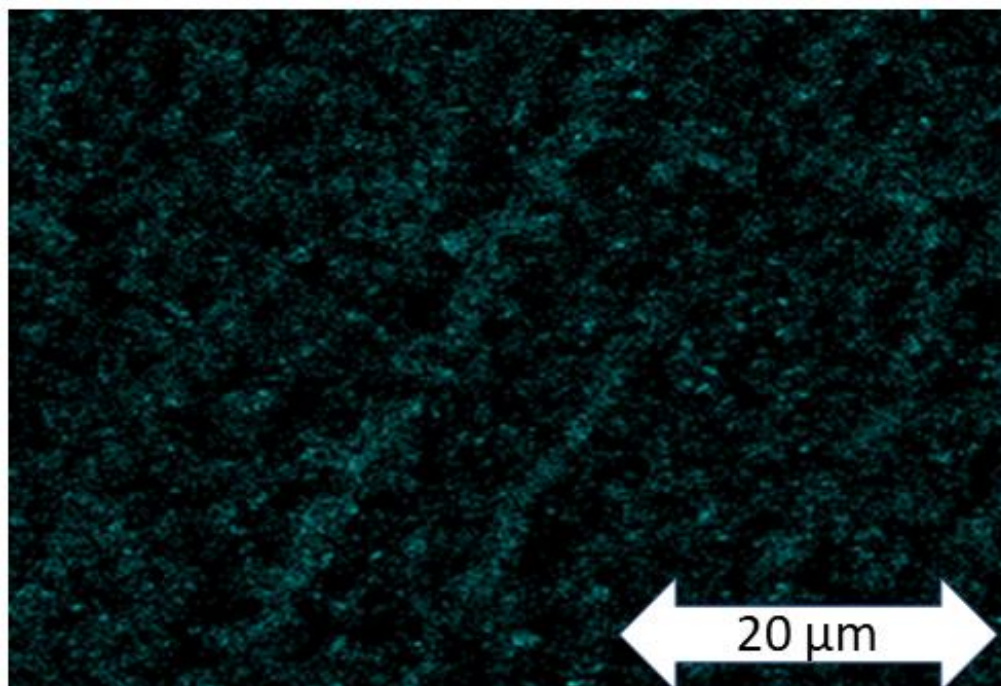


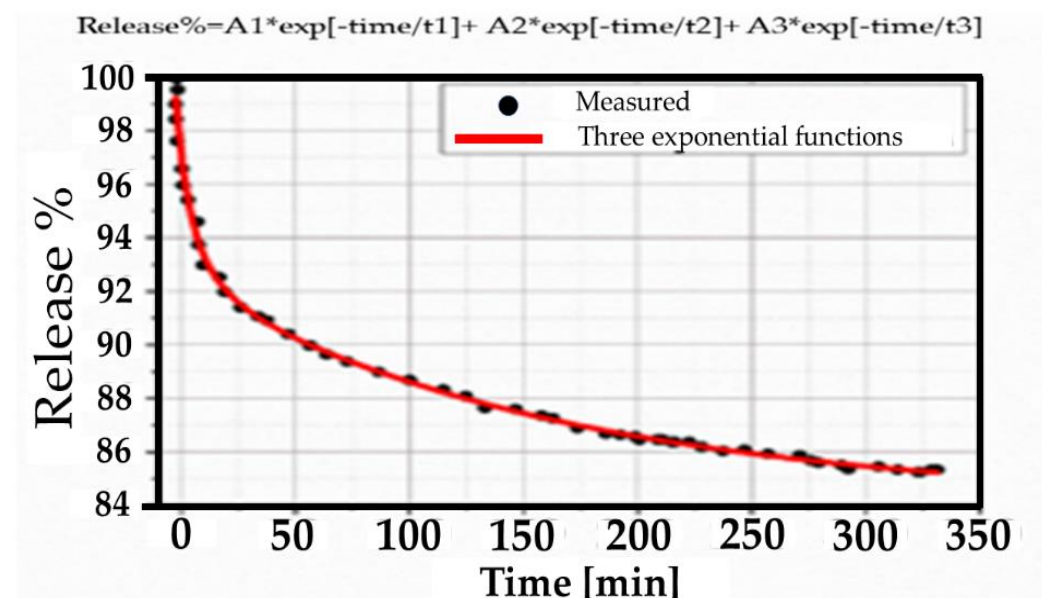
Figure 15. SEM mapping of the titanium element in the ORMOSIL coating on Mg ZK10-containing TiO_2 nanocontainers loaded with a 5-amino-1,3,4-thiadiazole-2-thiol (5-ATDT), indicating the homogeneous distribution of nanocontainers in the coating.

The literature documents many techniques as far as the encapsulation of corrosion inhibitors into the nanocontainers is concerned [144–146]. As for nanocontainers formed by coating a template and removing it by combustion, the most effective method is with the help of a vacuum chamber. One places a desired quantity of nanocontainers in a jar inside a chamber connected with a high vacuum pump. In a funnel that communicates with the chamber, one puts enough corrosion inhibitor diluted in a solvent. When a high vacuum in the chamber is observed and consequently transferred to the nanocontainers, one opens the funnel attached to the vacuum chamber, which floods the chamber. The adsorption of the corrosion inhibitor destroys the vacuum inside the nanocontainers. The amount encapsulated in nanocontainers is determined by the thermogravimetric analysis (TGA) method. One measures the weight of the same quantity as a function of the temperature in empty and full nanocontainers. The difference in weight resulting from these measurements is reduced by the lost weight of the encapsulated corrosion inhibitor. Table 2 shows the $w/w\%$ loading of inhibitors in TiO_2 , CeMo, and CeO_2 nanocontainers. The table shows that some corrosion inhibitors have a low loading on nanocontainers such as 8-HQ, regardless of the type. In other nanocontainers, the loading with corrosion inhibitors is large enough for one type, but the same nanocontainers do not accommodate a large amount of another corrosion inhibitor. Several reasons can explain this behavior related to the interaction or pore size of the nanocontainer with the corrosion inhibitor. It is a matter of optimization to find the best conditions for maximum loading. This fundamental result suggests that each system must specify this quantity to determine its effectiveness in CBCs before use. Brunauer–Emmett–Teller (BET) measurements can explain the physical adsorption of inhibitor molecules on a solid surface, pores, and the interior of the nanocontainers based on the critical analysis of their specific surface area [147].

Table 2. Inhibitor loading in the nanocontainers (Adapted with permission from Reference [148]).

Inhibitors	TiO ₂	CeMo	CeO ₂
8-hydroxyquinoline	3.56	5.22	5.22
5-amino-1,3,4-thiadiazole-2-thiol	18.90	46.45	21.91
2-mercaptobenzothiazole	6.14	59.44	63.42
1-H-benzotriazole-4-sulfonic acid	-	12.03	-
1-H-benzotriazole	-	-	54.17
p-toluenesulfonic acid	41.27	-	-

Developing the encapsulation technology of corrosion inhibitors in nanocontainers releases the active chemicals at a controlled rate in self-healing coatings. When the nanocontainers are ceramic, the corrosion inhibitor passes via the porous shell wall, assuming all are inside the nanocontainers. Here, the driving forces are the local pH change caused by corrosion, where they form polymers in the cracks of the CBC and heal it through chelation processes [149]. Therefore, one can suggest that the release rate depends on the thickness of the shell, permeability, distance from the crack, size of the crack, and the concentration of the nanocontainers. However, this simplified discussion is not accurate if Figure 16 measured the release of a corrosion inhibitor from nanocontainers [150]. The experimental curve was simulated by three equations indicating three kinetic release mechanisms from the nanocontainers, namely, fast (t_1), medium (t_2), and slow (t_3). At the beginning of the experiment, the corrosion inhibitors come from the surface of the nanocontainers. Later, the inhibitors in the walls participate in the release process. Finally, the inhibitors inside the shell take part in the release process. In other words, one can divide the corrosion inhibitors into three categories depending on their origin in the ceramic nanocontainers [150]. The release kinetics of 1-H-benzotriazole-4-sulfonic acid from the CeMo nanocontainers was fitted using three time constants [150].

**Figure 16.** Release of 8-HQ from CeMo nanocontainers with time (Adapted with permission from Ref. [150]).

This study shows that there are three types of corrosion inhibitions analogously that have enclaved, where their concentration depends on the volume of the nanoparticle. Suppose one assumes that the absorbance phenomena are independent of the nanocontainers' size for the same shell thickness. In that case, the corrosion inhibitions in the interior, pores,

and the surface of the nanocontainers are proportional to the internal volume, porosity volume, and surface area, respectively. The literature confirms this approach, proving experimentally that the degree of self-healing depends on the diameter of the microcontainer [151]. The maximum healing performance depends on the adequacy of the corrosion inhibitor to heal a specific size of the crack. Therefore, the design of the self-healing surface requires the actual quantity of inhibited corrosion agents, size of cracks, and endurance time of the self-healing coating for specific types of damage.

A second instrumental parameter that plays a substantial role in the self-healing of CBCs with corrosion inhibitor-loaded nanocontainers is their distance from the metal. An aluminum alloy AA2024-T3 was coated with two layers, A and B, where A was on the metal, and the B layer was on the A layer (Figure 17) [152]. Porous silicon nanocontainers (MBT@NCs) loaded with 2-mercaptobenzothiazole (MBT) inhibitor were loaded on the B-layer, and vice-versa in another experiment, namely, the A layer loaded with MBT@NCs. Increasing the distance between MBT@NCs and the metal surface benefits the barrier properties but worsens the corrosion inhibition. Inversely, this happens when MBT@NCs are incorporated into the coatings in direct contact in the future [152].

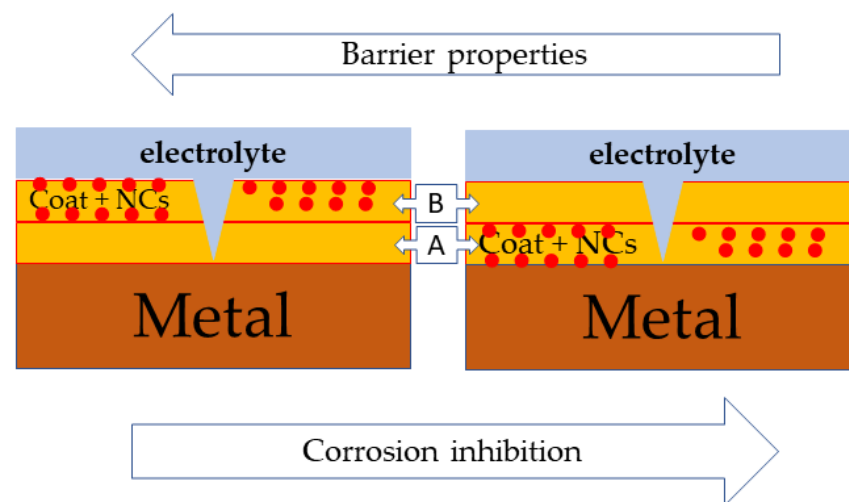


Figure 17. Two-layer coating of the same composition.

In another experiment, an aluminum alloy AA2024-T3 was coated with multiple surfaces containing CeMo(8-HQ) nanocontainers and others with nano-traps of water and chlorine (Figure 18) [153,154]. In one study, it was demonstrated that water traps drastically affected the diffusion coefficient of water in the ORMOSIL coatings [154].

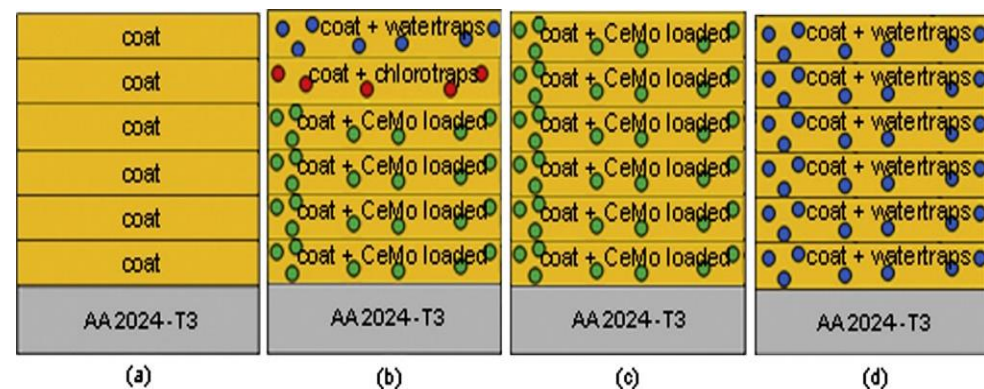


Figure 18. Samples consist of: (a) reference coating, (b) multifunctional coating, (c) inhibitor-loaded nanocontainers coating, and (d) water traps coating.

After producing CeMo nanocontainers, the pore diameter distribution was measured with the BET technique (Figure 19). From the analysis of isotherms (Figure 19a) from BET measurements, the mean pore radius was calculated to be 24.435 Å with a pore volume of 0.588 cm³/g (Figure 19b).

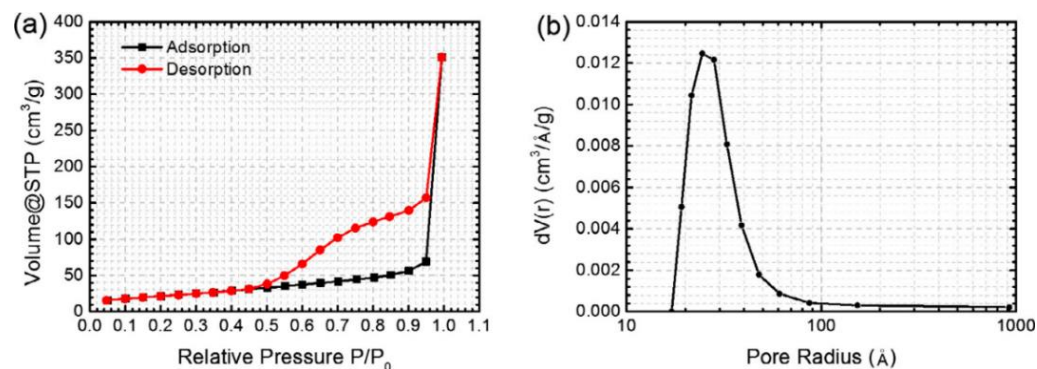


Figure 19. Evaluation of CeMo nanocontainers using BET: (a) adsorption and desorption isotherms and (b) pore size distribution.

These measurements are necessary to optimize nanocontainers for better exploitation to accommodate and release corrosion inhibitors. The multifunctional coatings (Figure 20) were loaded with CeMo(8-HQ) nanocontainers and coatings of water and chloride traps exposed to 0.5 M NaCl(aq) for 1 h, 144 h, and 288 h. Figure 20 shows the EIS Bode plots for these samples. From these measurements, the incorporation of traps and CeMo(8-HQ) is highly compatible with the coating ORMOSIL. EIS measurements show coatings to be highly effective in providing anticorrosion protection of metals, as shown by the high barrier properties. The addition of CeMo(8-HQ) and water and chloride traps improve the corrosion resistance of the CBCs amazingly.

SVET measurements demonstrated corrosion inhibition and the development of self-healing behavior. Furthermore, they studied the micromechanical properties of the CeMo(8-HQ)+nanotraps ORMOSIL coatings, showing that adding these pigments beneficially affects their mechanical properties [153].

Layered double hydroxides (LDHs) (Figure 21) are ionic layered solids consisting of hydroxide layer $[M^{II}_{1-x}M^{III}_x(OH)_2]^{x+}$ Z $[M^{II}_{1-x}M^{III}_x(OH)_2]^{x+}$ structures, where M represents the metal cations, and Z are layers of anions or/and neutral molecules (such as inhibitors, water, etc.). Z anions are softly attached and often replaceable. This property is used for self-healing purposes in cases of corrosion triggered by local changes in pH due to corrosion via an exchange between the inhibitor and hydroxyl anions [155]. The dimensions of polycrystalline particles range between 200 and 400 nm in length and the lateral size between 20 and 40 nm [156]. The incorporation of LDHs into a polymer coating loaded with divanadate anions as corrosion inhibitors were incorporated into a commercial primer on aluminum alloy 2024 [156]. The resulting CBCs exhibit a self-healing effect and give corrosion protection superior to that offered by CBCs on a chromium basis [156]. Furthermore, layered double hydroxides (LDHs) have been incorporated into CBCs executed for various functions. For example, in organic polymeric coatings, LDHs intercalated with nitrate anions act as chloride nanotraps [157]. Their occurrence in the coatings delays the diffusion of "chloride" ions to the metal surface and, consequently, the induction of corrosion processes. The literature makes extensive references to this system [96].

Another study reports the synergy between the layered double hydroxides (LDH) and cerium molybdate (CeMo) hollow nanocontainers incorporated into CBC, the anticorrosion properties of galvanized steel used in the automotive industry [158]. Both nanocontainers were loaded with MBT. The primer coating was loaded with LDH(MBT) or CeMo(MBT) in 4 wt.%. The third sample was produced combined with LDH(MBT) and CeMo(MBT) in a total amount equal to 4 wt.%. The electrochemical behavior was studied by EIS and SVET

techniques. Figure 22 shows the SVET results of total anodic and cathodic current obtained for the three coatings. One can perceive that the $I_{\text{anodic}} - I_{\text{cathodic}}$ are close to zero for up to 17 h for the LDH(MBT) sample, and then they start to increase linearly with the time. In the CeMo(MBT) sample, the $I_{\text{anodic}} - I_{\text{cathodic}}$ increases rapidly up to three hours due to corrosion and then drops to zero for times longer than 20 h due to self-healing.

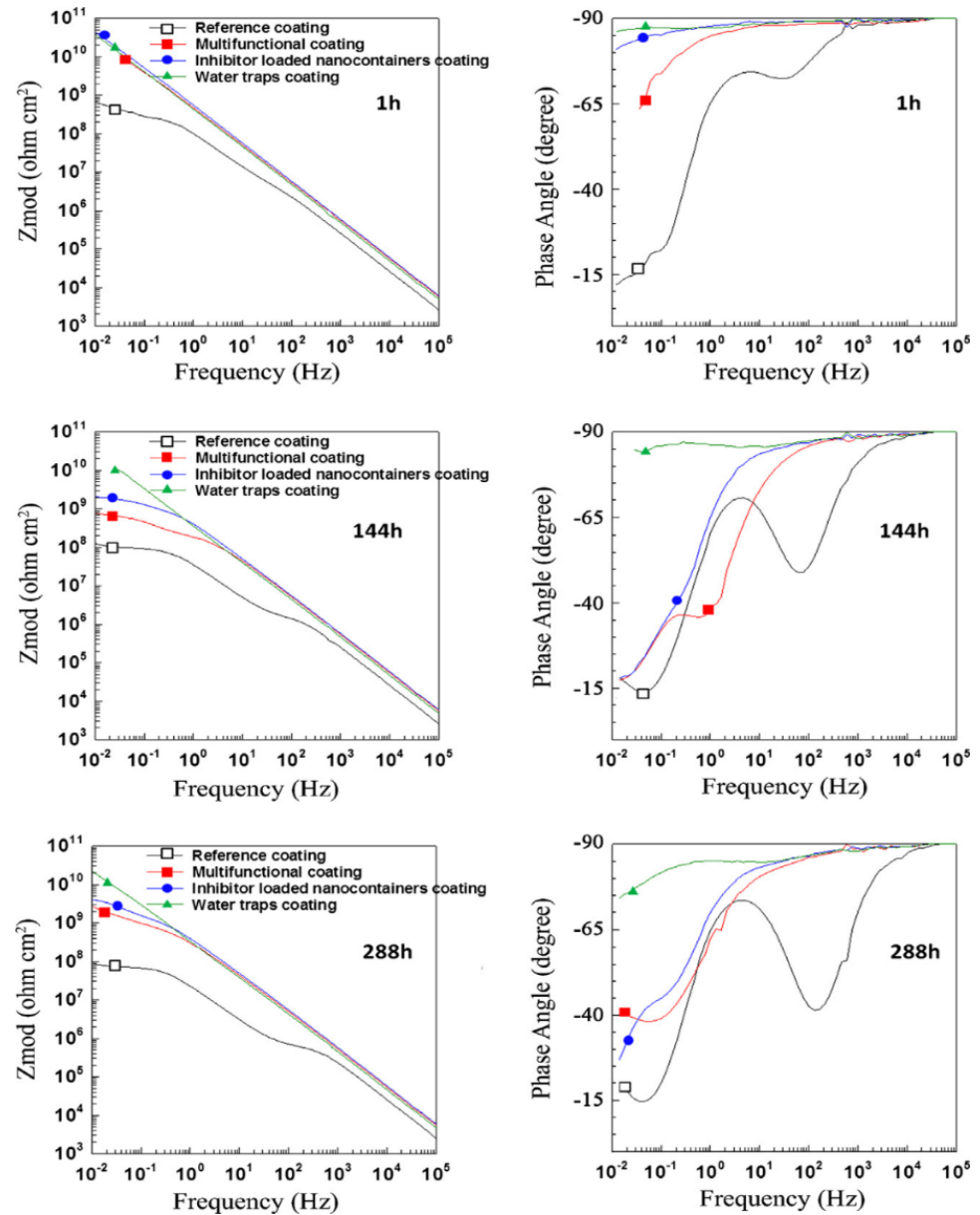


Figure 20. EIS Bode plots of the coatings exposed to 0.5 M NaCl(aq) for 1 h, 144 h, and 288 h.

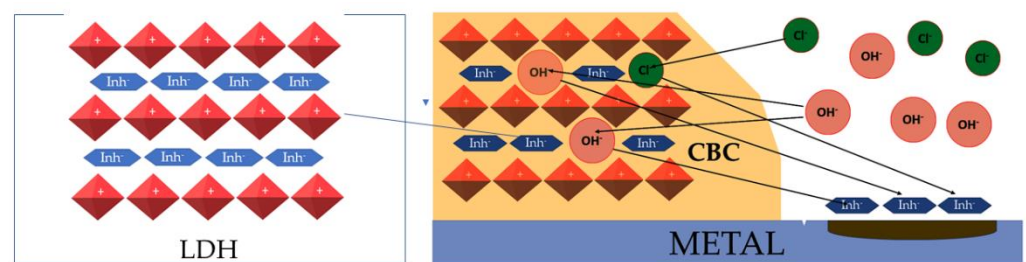


Figure 21. LDH nanocontainers act as a storage facility for inhibitors.

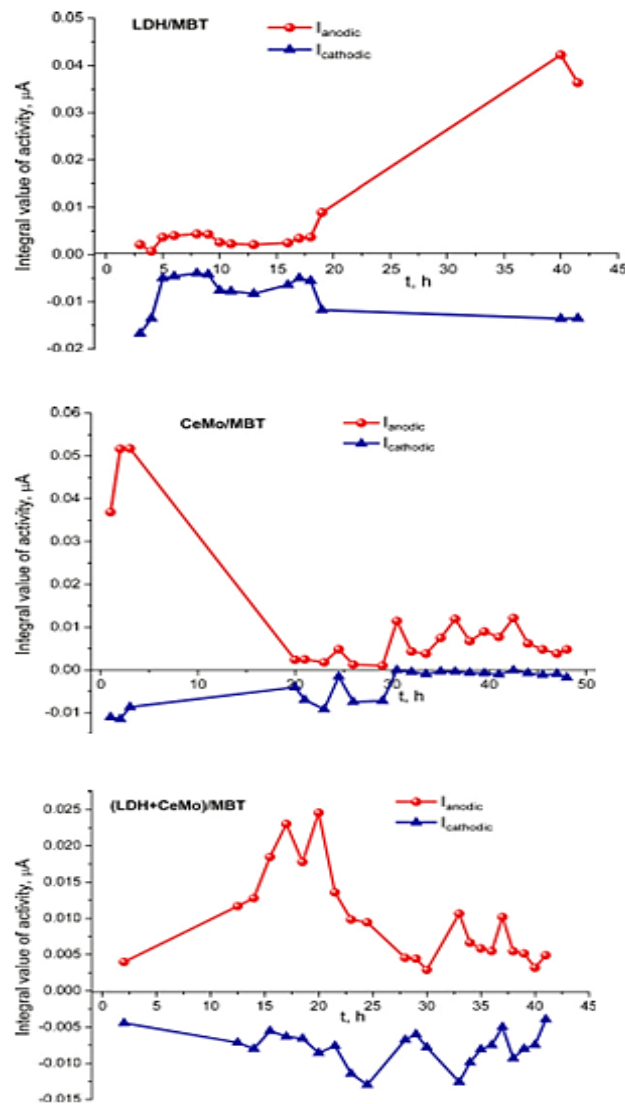


Figure 22. $I_{\text{anodic}} - I_{\text{cathodic}}$ current of the LDH(MBT), CeMo(LDH), and LDH(MBT) + CeMo (LDH) systems.

In the last sample consisting of LDH(MBT) + CeMo(MBT), $I_{\text{anodic}} - I_{\text{cathodic}}$ becomes maximal after 3–5 h of immersion in a salt solution. After that, both anodic and cathodic activities are low and do not exceed $5 \mu\text{A}/\text{cm}^2$, again due to self-healing. In summary, the inhibition of corrosion activity extends over a long period for the LDH(MBT) + CeMo(LDH) system. These results demonstrated a synergistic effect for corrosion inhibition and the self-healing effect by mixing the two nanocontainers [158].

The LbL system presents another approach to induce self-healing embedded in hybrid epoxy-functionalized $\text{ZrO}_2/\text{SiO}_2$ sol-gel coatings deposited onto the aluminum alloy AA2024 [159]. Here, 70 nm SiO_2 particles are multiple coated with poly(ethylene imine)/poly(styrene sulfonate) (PEI/PSS) polyelectrolyte layers. Benzotriazole (BTZ) is entrapped within the polyelectrolyte multilayers during the LbL-assembly. The pH changes during aluminum corrosion trigger the release of the inhibitor (BTZ). The LbL nano reservoir releases the stored inhibitor over a prolonged period of “on-demand” to damaged regions. The methodology appears to be cost-effective with active feedback on the corrosion processes. In another work, instead, SiO_2 particles produced ZnO particles coated with a polyaniline (PANI) polyelectrolyte layer. On it, they coated BZT, which enclaves with polyacrylic acid (PAA). The total particle size reached 950 nm. In this work, the release of BZT was measured with 3, 5, and 7 pH as a function of time. After 8 h, the BZT release

in $\text{mg L}^{-1}/\text{g}$ of ZnO nanocontainer at pH 3, 5, and 7 was 0.87, 0.59, and 0.36, respectively. LbL nanocarriers (5%) were incorporated into alkyd resin, and it was found after an electrochemical study that this system could be helpful for CBCs of marine interest [160]. Figure 23 makes the LbL technology more understandable to the reader.

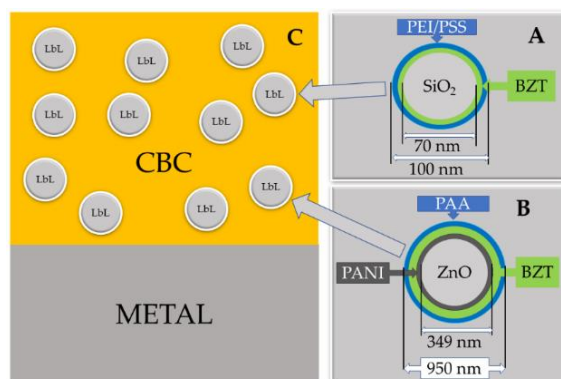


Figure 23. (A–C) Schematic representation of the SiO_2 and ZnO LbL technology.

In another study [161], the LbL particles were based on a cerium zinc molybdate (CZM) core coated with a PANI layer and polyelectrolyte layers mixed with an imidazole corrosion inhibitor. Studies determined the release of corrosion inhibitors as a function of pH and time. These LbL were incorporated into alkyd resins on mild steel and evaluated with electrochemical analysis (Tafel plot), where the improvement of their anticorrosion behavior was certified by incorporating LbL into the coating. In the two works [160,161], there is no discussion about whether these coatings offer the phenomenon of self-healing.

pH-Poly-(methacrylic acid) (PMAA)-sensitive nanocontainers (Figure 24) loaded with 2-MBT and hexafluoro titanate (H_2TiF_6) corrosion inhibitors significantly improved the anticorrosion properties of epoxy coatings on aluminum alloy 2024-T3, offering a beneficial effect on the anticorrosion properties of CBC [162].

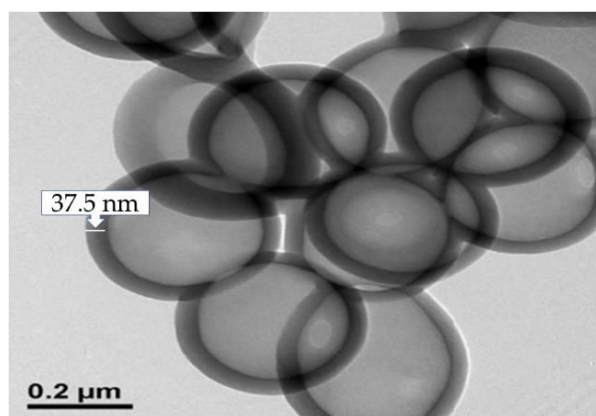


Figure 24. pH-Poly-(methacrylic acid) (PMAA)-sensitive nanocontainers.

Poly (methacrylic acid) (PMMA) and CeO_2 were combined to create PMAA@ CeO_2 nanocontainers filled with MBT and incorporated into an epoxy coating applied to an aerospace alloy (AA 2024-T3). The innovative coatings were examined with electrochemical impedance spectroscopy (EIS), and the results showed enhanced protection of the AA 2024-T3 substrate derived from the epoxy coating containing the 2-MBT-loaded nanocontainers [163].

Hollow mesoporous zirconia (hm-ZrO) nanospheres were prepared and charged with the 2-mercaptobenzothiazole corrosion inhibitor (2-MBT). Solid silicon nanoparticles as models were used to manufacture the ZrO shell after thermal solidification was removed

with NaOH. The nanocontainers had a size of 400 nm. The loading efficiency of 2-MBT was 63%. A 2-MBT release study was carried out for the nanocontainers, and it was found that its release was more remarkable in acidic and alkaline pH conditions than the neutral pH [164]. The same team produced hollow silicon spheres and loaded them with 2-MBT [165]. The 2-MBT kinetics was higher in the alkaline and acid environment than in the neutral pH. The silicon nanocontainers' inhibitor loading efficiency was more significant than that observed for hm-ZrO and was approximately 72%. The group went beyond the first study and incorporated these nanocontainers inside an organic-inorganic hybrid sol-gel coating made on modified 9Cr-1Mo ferrous steels. Active corrosion protection attributed to the releases of encapsulated inhibitor molecules was observed, thus demonstrating the "self-healing" ability of CS-NI [165].

Another more advanced system was developed consisting of hollow mesoporous silica nanocontainers (HMS) with molecular photo responsive switches such as azobenzene (AZO). The production started with the formation of SiO₂ templates coated by Azo-HMS, followed by the core removal. The containers were loaded with benzotriazole (BTA) released by light activation. The BTA@ Azo-HMS nanocontainers with light-responsive release properties were incorporated into an alkyd coating onto aluminum substrates. Upon UV irradiation, BTA was released, inducing self-healing [166].

Nano valves sensitive to pH were installed in the pores of the mesoporous silica nanoparticles (MSNs). Then, the nanocontainers were loaded with benzotriazole and incorporated into CBCs. Finally, the intelligent coatings were immersed in a 0.1 M NaCl solution; the EIS measurements were conducted at frequent time intervals. The impedance modulus of the blank metal decreased with the time up to 20 days of immersion in the salt solution. On the contrary, the impedance modulus of the coating with nanocontainers was $4.7 \times 10^4 \Omega \text{ cm}^2$ and $1.8 \times 10^5 \Omega \text{ cm}^2$ in 1 and 15 days, respectively. This increase with time was attributed to the "self-healing" effect [167].

So far, we have discussed spherical nanocontainers loaded with organic inhibitors. One group created halloysite nanotubes (HNTs) that charged them with cationic corrosion inhibitors such as Ce³⁺ and Zr⁴⁺ [168]. So far, such studies are rare in the literature [169]. The size of the pore of the nanotubes was 10 nm with a length ranging between 0.1 and 0.5 μm . There was an 80% reduction in the empty pore volume of HNT after filling with corrosion inhibitors in the lumen of the nanotubes. Coatings were created with the HNTs, and in this case, the "self-healing" effect was observed [168].

Multiwalled carbon nanotubes (MWCNTs) were loaded with benzimidazole (BZ) and incorporated into an epoxy coating. EIS and sacrificial tests evaluated the anticorrosion and self-healing properties of this coating. In addition, the impedance parameters were determined as a function of immersion time in a 3.5% NaCl solution up to 204 h. Based on the equivalent circuit describing the EIS measurements, the R_{film} parameters were determined to be $2.324 \times 10^4 \Omega \text{ cm}^2$, $2.605 \times 10^5 \Omega \text{ cm}^2$, and $8.365 \times 10^4 \Omega \text{ cm}^2$ for 12, 96, and 204 h of immersion in a salt solution, respectively. The increase of R_{film} up to 96 h was attributed to the "self-healing" effect. Following that time, the R_{film} parameter decreased due to inhibitor depletion from the MWCNTs [170].

Low-cost halloysite nanotubes from a commercial source were internally loaded with corrosion inhibitors (2-mercaptobenzothiazole) and then coated with multi-electrolyte hybrid strips. These modified nanotubes were incorporated into the coatings and studied for the protection provided against corrosion of the AA2024 aluminum alloy. Modified halloysite nanotubes do not allow the profuse release of the corrosion inhibitor (2-mercaptobenzothiazole), except on demand due to local pH changes that come from corrosion, and they appear to be a promising technology [171].

Attapulgite (ATP) nanoparticles were assembled with polyelectrolytes and BTA using the LbL technique. The fiber-shaped morphology of ATP was 0.8–1 μm long and 20 nm in diameter. Using multiple coating techniques, an ATP/polyethyleneimine (PEI)/poly(sodium-4-styrene sulfonate) (PSS)/benzotriazole (BTA)/poly(sodium-4-styrene sulfonate) (PSS)/benzotriazole (BTA) structure was manufactured and assessed via electrochemical methods.

The contact angle of water on CBC without the nanoparticles, the CNC with ATP, and the CBCs with the assembled ATP was equal to 68.8° , 73.3° , and 88.2° , respectively. The CBCs with the assembled ATP exhibit hydrophobicity, which is important for paints. Another important result presents the BTA release kinetics of the assembled ATP nanoparticle at pH = 7, 4, and 10, equal to 27.2, 34.7, and 86.4%, respectively. The release rates for pH equal to 7 and 4 are within the measurements' errors, indicating that the system is useless for an acidic environment. The EIS measurements were recorded as a function of time and analyzed using an equivalent circuit consisting of R_{sol} , R_{coat}/C_{coat} , and R_{ct}/CPE_{dl} . For 24 h of immersion in a salt solution, R_{coat} and R_{ct} were $9.5 \pm 0.20 \times 10^8$ and $2.1 \pm 0.44 \times 10^8$, respectively. For 384 h in a salt solution, R_{coat} and R_{ct} decreased down to $1.2 \pm 0.28 \times 10^8$ and $6.0 \pm 0.76 \times 10^7 \Omega \text{ cm}^2$, respectively. Indication for "self-healing" for the CBC-assembled ATP system was observed by scanning electrochemical microscopy (SECM), claimed by the same work [2].

To simulate a biomimetic network, self-healing coatings were manufactured in carbon steel to inhibit corrosion using cellulose nanofibers grafted with a corrosion inhibitor (oleic acid (OA)). Cellulose nanofibers have a terminal $-\text{OH}$ in the molecular chain where OA is attached and released from the fibers by changing the pH that causes the corrosion inhibitor to be desorbed from the nanofibers to cover the scratched metal providing protection, thus "self-healing" [172].

New generations of CBCs must be intelligent that attain this property from a new generation of nanocontainers incorporated into coatings exhibiting self-healing induced by pH, redox, temperature, light, and magnetic field. For example, the pores of mesoporous silica nanocontainers (HMS) were modified with azobenzene moieties. Azobenzene functioned as light switches that controlled the release of benzotriazole corrosion inhibitors (BTA). Resins on aluminum accommodated these light-sensitive nanocontainers. These CBCs automatically repair the corrosion area during ultraviolet radiation when scratched, where they release the corrosion inhibitors and aggravate the self-healing effect. The UV radiation at 365 nm modifies azobenzene in the cis form, so the pores open. However, when one illuminates visible light (450 nm), the azobenzene molecules that close the pores are irradiated with the pores because the isomer cis turns into trans, leading to the closure of the gates. As a result of this switching, the release kinetics of the erosion inhibitor from nanocontainers responds to radiations of 365 nm and 450 nm [173]. Similar CBC self-healing work has been done with microcapsules stimulated by sunlight [174]. In recent work, mesoporous silicon nanoparticles (MSNs) were surface-modified with tannic acid complexes that released the encapsulated benzotriazole corrosion inhibitor with pH triggering. The CBCs resulting from incorporating these MSNs into resins on metals exhibited self-healing after 20 days of immersion in a solution of 0.1 M NaCl, confirmed by electrochemical spectroscopy. The impedance modulus at 0.01 Hz grew from $4.7 \times 10^4 \Omega \text{ cm}^2$ to $1.8 \times 10^5 \Omega \text{ cm}^2$ after 15 days of immersion in the salt solution [167]. Another approach was made by developing nanocontainers that incorporate and release two corrosion inhibitors with different release mechanisms. 2-Mercaptobenzothiazole (MBT) inhibitor binds covalently to the nanocontainer shell [175]. Polydimethylsiloxane diglyceryl ether is incorporated inside the nanocontainers. MBT first releases from the nano permeable shell that allows the release of the packaged inhibitor and eventually leads to the sequential release of the two inhibitors. This new methodology is in its infancy, but it is very promising [175].

The development of supramolecular chemistry has widened the scope for manufacturing smart containers by installing supramolecular nano valves into their pores [176]. The exterior of the $\text{Fe}_3\text{O}_4@m\text{SiO}_2$ nanocontainer incorporated supramolecular assemblies of hypiridynium c water soluble pillar(5)arenes, thus creating corrosion potential stimulus-responsive gates. The supramolecular gate keepers engulfed the encapsulated 8-hydroxyquinoline, a corrosion inhibitor, within the $\text{Fe}_3\text{O}_4@m\text{SiO}_2$ nanocontainers embedded in resins on AZ31B. These innovative coatings demonstrate the phenomenon of self-healing by creating a protective layer on the magnesium stimulated by corrosion potential [177].

12. Corrosion Sensors

The destruction of CBCs can be caused by cracks in the metal or by corrosion. All these adversities must be sensed immediately to obtain measures to protect the metal structure. The automatic diagnosis of these damages reduces the cost of repairs and increases construction safety, especially in airplanes. Corrosion in airplanes can occur in inaccessible places and is extremely difficult to find. Faults can be diagnosed visually by relatively simple corrosion inspection, e.g., with colored products resulting from local change in pH or automated electronic mechanization. Another automation that should be added to airplane metal structures is that of anti-icing for the automatic removal of ice from its wings.

A technique used in a steel and aluminum paint star system is fluorescent corrosion (FCI) used in paint and coating primer systems for steel and aluminum alloys.

7-Diethylamine-4-methylcoumarin (7-DMC) (indicator, coumarin derivative) was added in amounts of about 0.05 to 1.5 wt% in the epoxy/polyamide primer stained on the alloy substrate. After this primer, they passed the epoxy top polyamide overcoat. Each dye had a thickness of 30 microns. Indicators change color or fluorescence depending on the pH or changes in the oxidation state of the metal [178,179].

Lumogallion, *N,N*-bis-(salicylidene)-2,3-diaminobenzofuran (SABF), and Phen Green™ were incorporated into epoxy/polyamide primer to determine how aqueous solution and corrosion processes affect the Al^{3+} , Mg^{2+} , and Cu^{2+} ions. Fluorescence microscopy was employed to identify the localized corrosion and corrosion processes occurring. In conclusion, they have shown that fluorescent probes respond to changes in metal ions Al^{3+} , Mg^{2+} , and Cu^{2+} in an aqueous solution [180].

3',6'-Bis (diethylamino)-2-[(1-methyl)amine] ("FD1") was incorporated into epoxy coatings for the timely detection of steel corrosion. Steel corrosion products stimulated the FD1 index, and fluorescence prematurely identified them when mixed with the coating precursors in the anode region during steel corrosion. This method can be considered an early corrosion detection method created in steels for timely diagnosis before the metal is severely damaged [181].

Various pH-sensitive microcapsules containing corrosion indicators were synthesized and incorporated into commercially available coatings. The indicators were bromothymol blue, phenol red, neutral red, cresol red, and phenolphthalein blue, coloring the coatings purple, yellow, reddish-purple, and fuchsia, respectively. Preliminary results from salt fog testing of prototypes showed that pH-sensitive microcapsules detect corrosion before visible rust appears, even in hidden areas [182].

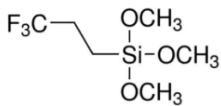
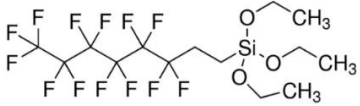
Coumarin was chosen as a fluorescent index (FI) incorporated into coatings to monitor the underlying corrosion on various metal substrates where corrosion reactions change the pH [183]. Coumarin initially fluoresces in ultraviolet light but changes to non-fluorescent at the corrosion point. This was used to estimate the corrosion reactions between the metal and the coating. This was associated with the change in fluorescence intensity of the coating. The coating was immersed in a 3.5% sodium chloride solution and examined after 24 h for corrosion sites caused by pH. The energy dispersion spectroscopy of selected samples proved that fluorescence reduction was associated with corrosion points. The method showed that the optimal thickness of the coating is 80 μm . Fi in the coating system can reveal corrosion under specially prepared coatings before any visible damage occurs on the surface of the coating itself [183].

Phenolphthalein (PhPh) was loaded into silica nanocontainers (SiNC) to form efficient pH sensors for early corrosion detection of polymer matrix on AZ31 [184]. The color of PhPh changes to pink upon local corrosion that is observable by visual inspection. The system also exhibited "self-healing". The investigators noted that their system at the micron range could detect minor corrosion events. With this pH sensitivity via drastic color-signaling, the service life of the metallic structures can increase, yielding a reduction in maintenance costs, combined with frequent inspections [184].

Silicium nanocontainers loaded with phenolphthalein were incorporated into resins of the company Mankiewicz GmbH (Germany) on aluminum and magnesium metals. These coatings were designed to detect pH changes resulting from corrosion via local color change resulting from the interaction of phenolphthalein in active cathodic regions. The tests demonstrate the pH sensitivity of advanced nanomaterials dispersed in aqueous solutions. Experiments have shown that this system may be suitable for corrosion detection [185].

(3-Glycidyloxypropyl) trimethoxy silane (GPTMS), methyltrimethoxysilane (MTMS), and hexamethylmethoxymelamine (HMMM) were crosslinked with FAS-3 (3,3,3-trifluoropropyltrimethoxysilane) and FAS-17(1H,1H,2H,2H-perfluorodecyltriethoxysilane) (Table 3) to create a hydrophobic coating of thickness two μm on aluminum metal heated in an oven in 120 °C for 30 min [186]. The coating had enhanced hydrophobicity with an angle of contact of approximately 120°. The coatings were studied with potentiodynamic polarization and electrochemical paralysis (EIS), which showed reduced corrosion associated with water-repellence and an intersecting network of low cross-permeability [186].

Table 3. Compounds inducing superhydrophobicity.

FAS-3 (3,3,3-trifluoropropyltrimethoxysilane)	
FAS-17 (1H,1H,2H,2H-perfluorodecyltriethoxysilane)	

The coatings made have the rough morphology, as depicted in Figure 25. Such an interface with entrapped air between metal and electrolyte prevents Cl^- ions from reacting with the metal substrate. In addition, the air valleys formed are occlusive, thus increasing the corrosion resistance. Another hypothesis is that the dense, net barrier of the epoxy–HMMM hybrid structure results in a strong adhesion with aluminum metal oxide with hydrophobic groups of perfluoro pointing outwards, making water and Cl^- water molecules challenging to penetrate [186].

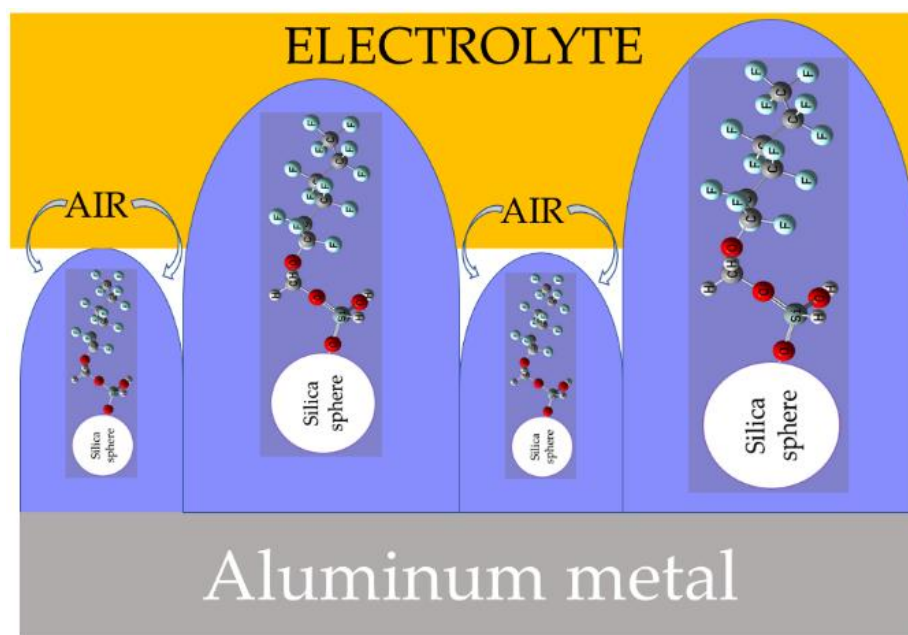


Figure 25. Model of an interface between the superhydrophobic and salt solution to explain the increased resistance to corrosion and hydrophobicity.

13. Conclusions with Perspectives

The last twenty years have realized remarkable achievements in terms of CBCs' investigation techniques and the creation of chemistries for remarkable CBC performances. However, giant leaps have been made to develop active CBCs with nanocontainers of different types, shapes, responses, and aptitudes. Nevertheless, many challenges continue to be endemic in science and the technology of passive and active CBCs, and we are waiting for an exciting period of future research. The main challenges focus on developing multifunctional micro/nano-containers that can accommodate various corrosion inhibitors that will activate on-demand, the development of new nanocontainers of small size but large load capacity, and their compatibility with commercial resins. What we avoid discussing in the literature is what are the requirements of the industry and what should be the performances of these new protective coatings. The question arises of the "industry requirements" for such CBCs.

The new CBCs should be standardized according to their implementation. The only stakes should not be the replacement of chrome with environmentally friendly processes but the extension of the life of the protection offered by the current CBCs. As far as the car industry is concerned, we must beware of the increase in time of corrosion protection for light alloys (aluminum, magnesium), which allows for higher car production use. As far as steel is concerned, the aim is to exceed the ASTM B117 [187], which is 500 h of protection in a salt spray chamber, and to double it. Innovative technology must protect their resistance to scratches, graffiti, and exposure to water. The requirements of modern technology are entirely different in aeronautics. It is a well-known fact that we achieve approximately three thousand hours of salt spraying testing with chromate technology. If we want to classify a new "self-healing" CBC technology as successful, we must double the current maintenance intervals to save their maintenance cost. The new systems to be achieved by the prolonged release of healing agents must also be multifunctional, and in the case of airplanes, a critical activity is anti-icing.

In the case of aeronautics, there is a great need to develop CBCs, which, with some automation of the status of CBCs, can consolidate the condition of the coating. The third objective is the shipping industry; in this case, it is necessary to double the lifespan of existing coating systems. The "self-healing" of CBCs will bring additional benefits. The discovery of new biocides derived from nature and included in eco-technology is imperative to remove the harmful biocides we use today. Today, we are seeing much work to find new nano-containers and new coating CBCs. However, this is not enough, considering that the industries that will use these products are cautious in approaching the new proposed solutions. The literature has a few examples that follow different approaches.

For example, Zn/Al LDH manufactured by anion exchange was used in an EADS primer for aeronautical application and offered a masterful self-healing effect. Electrochemical and enhanced corrosion tests have established this. Developed LDH nanocontainers are promising applicants for the replacement of chromate-based anticorrosion pigments, as they provide comparable or even more excellent corrosion protection properties [156]. Another example comes from the maritime industry. Here, CuO, ZnO, and CeMo nanocontainers were loaded with bromosphaerol (CuO and ZnO), and 8-hydroxyquinoline (CeMo) was incorporated into commercial paints used by Wilkens SA and Re-Turn SA, and two ships were painted to test the technology in seawater. Bromosphaerol comes from the marine environment and is an essential ecological biocide. The ship painted with Wilkens SA paints traveled across the Adriatic Sea, and the other ship painted with the Re-Turn paint traveled around the world, both at 14 knots. After a year, the two ships were taken out from the seawater and inspected for fouling and corrosion. The inspection found that the nanotechnology-painted stripes were in better condition than the same commercial paints used for the rest of the ships [40,188–191]. Here, it is important to note that large quantities of nanocontainers were produced in pilot-scale production, indicating that our technology can quickly pass on to industrial-scale production. The quantities of copper and CeMo are minimal. The bromosphaerol comes from a *Ficus* from the sea near Corfu

and is grown in a nursery to obtain large quantities. This technology is ecological, and there is no need for licenses to apply it to ships.

Research and development of “self-healing” CBCs have reached enormous magnitudes globally, involving many academic and industrial research organizations. The sponsorship by state and industrial organizations increases over time strongly with an incentive not only to understand the mechanisms of healing but to create some new products. There are a few commercial successes, such as Nissan’s “Scratch Guard Coat” painting system [192]. However, the road is very long because the time from developing a prototype until it comes into production is very long. Nevertheless, this does not prevent the government and the industrial finance organizations from increasing investment because the incentives are plentiful, such as reducing the cost of maintenance and repair of CBCs, especially in remote construction sites. This article has an incentive to review the literature so that it becomes an open discussion of the state of the art and the steps that need to be done to soon have commercial applications. “Self-healing” materials have huge boundaries for increasing the resistance of CBCs to corrosion. There is considerable scope for developing new materials such that these sensors will detect the corrosion onsets automatically. We have many creative years ahead of us to work in this beautiful field of self-healing materials that will be readily available for our everyday uses one day soon.

Funding: Support by the grant Self-Healing Construction Materials (contract No. 075-15-2021-590 dated 4 June 2021) is greatly appreciated.

Institutional Review Board Statement: Not applicable.

Informed Consent Statement: Not applicable.

Data Availability Statement: Not applicable.

Acknowledgments: The author is thankful for support from the grant Self-Healing Construction Materials (Contract Nos. 075-15-2021-590 dated 4 June 2021). The author also thanks M.R. Sanjay (Natural Composites Research Group Lab, Department of Materials and Production Engineering, The Sirindhorn International Thai German Graduate School of Engineering (TGGS), King Mongkut’s University of Technology, North Bangkok (KMUTNB), Bangkok, Thailand) for proofreading the manuscript. I dedicate this Review Article to the memory of the late friend and collaborator, George Edward Thompson, who worked together in the FP6 MULTIPROTECT (Advanced environmentally friendly multifunctional corrosion protection by nanotechnology) program for many years, and we exchanged many scientific ideas and personal conversations.

Conflicts of Interest: There is no conflict of interest.

References

1. Park, R.M.; Bena, J.F.; Stayner, L.T.; Smith, R.J.; Gibb, H.J.; Lees, P.S.J. Hexavalent chromium and lung cancer in the chromate industry: A quantitative risk assessment. *Risk Anal.* **2004**, *24*, 1099–1108. [[CrossRef](#)] [[PubMed](#)]
2. Liu, X.; Zhang, D.; Hou, P.; Pan, J.; Zhao, X.; Hou, B. Preparation and Characterization of Polyelectrolyte-Modified Attapulgite as Nanocontainers for Protection of Carbon Steel. *J. Electrochem. Soc.* **2018**, *165*, C907–C915. [[CrossRef](#)]
3. Chen, D.; Ray, A.K. Removal of toxic metal ions from wastewater by semiconductor photocatalysis. *Chem. Eng. Sci.* **2001**, *56*, 1561–1570. [[CrossRef](#)]
4. Hoffmann, L.; Grinderslev, M. *Mass Flow Analysis of Chromium and Chromium Compounds*; Environmental Project, No. 793; The Danish Environmental Protection Agency: Copenhagen, Denmark, 2003.
5. Authorisation and Restriction of Chemicals (REACH). 1907/2006 (*Regula*); Repealing Council Regulation (EEC) No 793/93 and Commission Regulation (EC) No 1488/94; EU-OSHA: Brussels, Belgium, 2006.
6. European Commission. *Amending 340/2008*; L 139/1; EU-OSHA: Brussels, Belgium, 2018; Volume 2016.
7. Qi, J. Trivalent Chromium Conversion Coatings on Al and Al-Cu Alloys. PhD Thesis, The University of Manchester, Manchester, UK, 2015.
8. Qi, J.; Gao, L.; Li, Y.; Wang, Z.; Thompson, G.E.; Skeldon, P. An Optimized Trivalent Chromium Conversion Coating Process for AA2024-T351 Alloy. *J. Electrochem. Soc.* **2017**, *164*, C390–C395. [[CrossRef](#)]
9. Guo, Y.; Frankel, G.S. Active corrosion inhibition of AA2024-T3 by trivalent chrome process treatment. *Corrosion* **2012**, *68*, 045002-1–045002-10. [[CrossRef](#)]
10. Guo, Y.; Frankel, G.S. Characterization of trivalent chromium process coating on AA2024-T3. *Surf. Coat. Technol.* **2012**, *206*, 3895–3902. [[CrossRef](#)]

11. Santa Coloma, P.; Izagirre, U.; Belaustegi, Y.; Jorcin, J.B.; Cano, F.J.; Lapeña, N. Chromium-free conversion coatings based on inorganic salts (Zr/Ti/Mn/Mo) for aluminum alloys used in aircraft applications. *Appl. Surf. Sci.* **2015**, *345*, 24–35. [CrossRef]
12. Chidambaram, D.; Clayton, C.R.; Halada, G.P. The role of hexafluorozirconate in the formation of chromate conversion coatings on aluminum alloys. *Electrochim. Acta* **2006**, *51*, 2862–2871. [CrossRef]
13. Qi, J.T.; Hashimoto, T.; Walton, J.R.; Zhou, X.; Skeldon, P.; Thompson, G.E. Trivalent chromium conversion coating formation on aluminium. *Surf. Coat. Technol.* **2015**, *280*, 317–329. [CrossRef]
14. Corporation, H.; Heights, M.; States, U.; Corporation, H.C.; Capital, H.; Interlomas, C.U.; Huller, R.K.; District, N. *Henkel Ready-to-Use Surface Treatments for the Aerospace Industry*; Henkel: Dusseldorf, Germany, 2018; Volume 8340.
15. Socomore. “Socosurf TCS.” Aluminum Surface Treatment. Available online: <https://www.socomore.com/en/contact-us> (accessed on 18 April 2022).
16. Pearlstein, F.; Agarwala, V.S. Trivalent chromium solutions for applying chemical conversion coatings to aluminum alloys or for sealing anodized aluminum. *Plat. Surf. Finish.* **1994**, *81*, 50–55.
17. Li, L.; Swain, G.M. Formation and structure of trivalent chromium process coatings on aluminum alloys 6061 and 7075. *Corrosion* **2013**, *69*, 1205–1216. [CrossRef]
18. Qi, J.; Gao, L.; Liu, Y.; Liu, B.; Hashimoto, T.; Wang, Z.; Thompson, G.E. Chromate Formed in a Trivalent Chromium Conversion Coating on Aluminum. *J. Electrochem. Soc.* **2017**, *164*, C442–C449. [CrossRef]
19. Qi, J.; Światowska, J.; Skeldon, P.; Marcus, P. Chromium valence change in trivalent chromium conversion coatings on aluminium deposited under applied potentials. *Corros. Sci.* **2020**, *167*, 108482. [CrossRef]
20. Eastmond, D.A.; MacGregor, J.T.; Slesinski, R.S. Trivalent chromium: Assessing the genotoxic risk of an essential trace element and widely used human and animal nutritional supplement. *Crit. Rev. Toxicol.* **2008**, *38*, 173–190. [CrossRef] [PubMed]
21. Ambreen, K.; Khan, F.H.; Bhadauria, S.; Kumar, S. Genotoxicity and oxidative stress in chromium-exposed tannery workers in North India. *Toxicol. Ind. Health* **2014**, *30*, 405–414. [CrossRef]
22. Blasiak, J.; Kowalik, J. A comparison of the in vitro genotoxicity of tri- and hexavalent chromium. *Mutat. Res.-Genet. Toxicol. Environ. Mutagen.* **2000**, *469*, 135–145. [CrossRef]
23. Speetjens, J.K.; Collins, R.A.; Vincent, J.B.; Woski, S.A. The nutritional supplement chromium(III) tris(picolinate) cleaves DNA. *Chem. Res. Toxicol.* **1999**, *12*, 483–487. [CrossRef]
24. Stearns, D.M.; Wise, J.P.; Patierno, S.R.; Wetterhahn, K.E. Chromium(III) picolinate produces chromosome damage in Chinese hamster ovary cells. *FASEB J.* **1995**, *9*, 1643–1648. [CrossRef]
25. Coryell, V.H.; Stearns, D.M. Molecular analysis of hprt mutations induced by chromium picolinate in CHO AA8 cells. *Mutat. Res.-Genet. Toxicol. Environ. Mutagen.* **2006**, *610*, 114–123. [CrossRef]
26. Wang, C.; Jiang, F.; Wang, F. Cerium chemical conversion coating for aluminum alloy 2024-T3 and its corrosion resistance. *Corrosion* **2004**, *60*, 237–243. [CrossRef]
27. Giles, T.R.; Vonk, D.; Favero, S.-L. The Next Generation of Conversion Coatings. In Proceedings of the Encontro e Exposição Brasileira de Tratamento de Superfície III INTERFINISH Latino Americano, São Paulo, Brazil, 11–14 April 2012; pp. 172–181.
28. Kapic, E.; Heights, S.; Goodreau, B.H.; Romeo; Bobadilla, A.; Oak, R.; Febraro, M.; Knoxville, T. Processes and Compositions for Improving Corrosion Performance of Zirconium Oxide Pretreated Zinc Surfaces. US Patent 9,573,162, 21 February 2017.
29. Vonk, D.R.; Kapic, E.; Sienkowski, M.L. Metal Pretreatment Composition Containing Zirconium, Copper, and Metal Chelating Agents and Related Coatings on Metal Substrates. US Patent 9,284,460, 15 March 2016.
30. Matsukawa, M.; Shi, N.; Makino, K.; Shi, Y.; Toshiaki Shimakura, I. Chemical Conversion Coating Agent and Surface-Treated Metal. U.S. Patent US7510612B2, 31 March 2009.
31. Šekularac, G.; Milošev, I. Electrochemical Behavior and Self-Sealing Ability of Zirconium Conversion Coating Applied on Aluminum Alloy 3005 in 0.5 M NaCl Solution. *J. Electrochem. Soc.* **2020**, *167*, 021509. [CrossRef]
32. Doerre, M.; Hibbitts, L.; Patrick, G.; Akafuah, N.K. Advances in automotive conversion coatings during pretreatment of the body structure: A review. *Coatings* **2018**, *8*, 405. [CrossRef]
33. Milošev, I.; Frankel, G.S. Review—Conversion Coatings Based on Zirconium and/or Titanium. *J. Electrochem. Soc.* **2018**, *165*, C127–C144. [CrossRef]
34. Peng, D.; Wu, J.; Yan, X.; Du, X.; Yan, Y.; Li, X. The formation and corrosion behavior of a zirconium-based conversion coating on the aluminum alloy AA6061. *J. Coat. Technol. Res.* **2016**, *13*, 837–850. [CrossRef]
35. Asemani, H.R.; Ahmadi, P.; Sarabi, A.A.; Eivaz Mohammadloo, H. Effect of zirconium conversion coating: Adhesion and anti-corrosion properties of epoxy organic coating containing zinc aluminum polyphosphate (ZAPP) pigment on carbon mild steel. *Prog. Org. Coat.* **2016**, *94*, 18–27. [CrossRef]
36. Taheri, P.; Laha, P.; Terryn, H.; Mol, J.M.C. An in situ study of zirconium-based conversion treatment on zinc surfaces. *Appl. Surf. Sci.* **2015**, *356*, 837–843. [CrossRef]
37. Gray, J.E.; Luan, B. Protective coatings on magnesium and its alloys—A critical review. *J. Alloys Compd.* **2002**, *336*, 88–113. [CrossRef]
38. Šekularac, G.; Kovač, J.; Milošev, I. Prolonged protection, by zirconium conversion coatings, of AlSi7Mg0.3 aluminium alloy in chloride solution. *Corros. Sci.* **2020**, *169*, 108615. [CrossRef]
39. Golru, S.S.; Attar, M.M.; Ramezanzadeh, B. Morphological analysis and corrosion performance of zirconium based conversion coating on the aluminum alloy 1050. *J. Ind. Eng. Chem.* **2015**, *24*, 233–244. [CrossRef]

40. Kordas, G. Nanocontainers Against Biofouling and Corrosion Degradation of Materials: A Short Review With Prospects. *Front. Nanotechnol.* **2022**, *4*, 813908. [[CrossRef](#)]
41. Díaz, B.; Härkönen, E.; Światowska, J.; Maurice, V.; Seyeux, A.; Marcus, P.; Ritala, M. Low-temperature atomic layer deposition of Al₂O₃ thin coatings for corrosion protection of steel: Surface and electrochemical analysis. *Corros. Sci.* **2011**, *53*, 2168–2175. [[CrossRef](#)]
42. Garg, R.; Rajagopalan, N.; Pyeon, M.; Gönüllü, Y.; Fischer, T.; Khanna, A.S.; Mathur, S. Plasma CVD grown Al₂O₃ and MgAl₂O₄ coatings for corrosion protection applications. *Surf. Coat. Technol.* **2018**, *356*, 49–55. [[CrossRef](#)]
43. Wang, D.; Bierwagen, G.P. Sol-gel coatings on metals for corrosion protection. *Prog. Org. Coat.* **2009**, *64*, 327–338. [[CrossRef](#)]
44. Figueira, R.B.; Silva, C.J.R.; Pereira, E.V. Organic–inorganic hybrid sol–gel coatings for metal corrosion protection: A review of recent progress. *J. Coat. Technol. Res.* **2015**, *12*, 1–35. [[CrossRef](#)]
45. Catubig, R.; Hughes, A.E.; Cole, I.S.; Hinton, B.R.W.; Forsyth, M. The use of cerium and praseodymium mercaptoacetate as thiol-containing inhibitors for AA2024-T3. *Corros. Sci.* **2014**, *81*, 45–53. [[CrossRef](#)]
46. Ahamad, I.; Prasad, R.; Quraishi, M.A. Thermodynamic, electrochemical and quantum chemical investigation of some Schiff bases as corrosion inhibitors for mild steel in hydrochloric acid solutions. *Corros. Sci.* **2010**, *52*, 933–942. [[CrossRef](#)]
47. Kartsonakis, I.A.; Balaskas, A.C.; Kordas, G.C. Influence of cerium molybdate containers on the corrosion performance of epoxy coated aluminium alloys 2024-T3. *Corros. Sci.* **2011**, *53*, 3771–3779. [[CrossRef](#)]
48. Zheludkevich, M.; Tedim, J.; Ferreira, M. “Smart” coatings for active corrosion protection based on multi-functional micro and nanocontainers. *Corros. Sci.* **2015**, *82*, 314–323. [[CrossRef](#)]
49. Wang, T.; Du, J.; Ye, S.; Tan, L.; Fu, J. Triple-Stimuli-Responsive Smart Nanocontainers Enhanced Self-Healing Anticorrosion Coatings for Protection of Aluminum Alloy. *ACS Appl. Mater. Interfaces* **2019**, *11*, 4425–4438. [[CrossRef](#)]
50. Malinskii, Y.M.; Prokopenko, V.; Ivanova, N.; Kargin, V. A Investigation of Self-Healing of Cracks in Polymers. *Mekhanika Polim.* **1970**, *2*, 271–275.
51. Wool, R.P. Material response and reversible cracks in viscoelastic polymers. *Polym. Eng. Sci.* **1978**, *18*, 1057–1061. [[CrossRef](#)]
52. Wool, R.P.; O’Connor, K.M. A theory crack healing in polymers. *J. Appl. Phys.* **1981**, *52*, 5953. [[CrossRef](#)]
53. White, S.R.; Sottos, N.R.; Geubelle, P.H.; Moore, J.S.; Kessler, M.R.; Sriram, S.R.; Brown, E.N.; Viswanathan, S. Autonomic Healing of Polymer Composites. *Nature* **2001**, *409*, 794. [[CrossRef](#)] [[PubMed](#)]
54. Brinker, C.J.; Scherer, G.W. *Sol-Gel Science The Physics and Chemistry of Sol-Gel Processing*; Academic Press, Inc.: Boston, UK, 1990; ISBN 978-0-12-134970-7.
55. Brinker, C.J. Hydrolysis and condensation of silicates: Effect on structure. *J. Non. Cryst. Solids* **1998**, *100*, 31–50. [[CrossRef](#)]
56. Innocenzi, P.C.; Guglielmi, M.; Gobbin, M.; Colombo, P. Coating of metals by the sol-gel dip-coating method. *J. Eur. Ceram. Soc.* **1992**, *10*, 431–436. [[CrossRef](#)]
57. Deflorian, F.; Rossi, S.; Fedel, M.; Ecco, L.G.; Paganica, R.; Bastarolo, M.; Mathiazhagan, A.; Joseph, R.; Chen, X.; Hong, R.; et al. Corrosion protection properties of organofunctional silanes—An overview. *Prog. Org. Coat.* **2005**, *51*, 259–269.
58. Palomino, L.M.; Suegama, P.H.; Aoki, I.V.; Fatima Montemor, M.; De Melo, H.G. Electrochemical study of modified non-functional bis-silane layers on Al alloy 2024-T3. *Corros. Sci.* **2008**, *50*, 1258–1266. [[CrossRef](#)]
59. Montemor, M.F.; Cabral, A.M.; Zheludkevich, M.L.; Ferreira, M.G.S. The corrosion resistance of hot dip galvanized steel pretreated with Bis-functional silanes modified with microsilica. *Surf. Coat. Technol.* **2006**, *200*, 2875–2885. [[CrossRef](#)]
60. Franquet, A.; Biesemans, M.; Willem, R.; Terryn, H.; Vereecken, J. Multinuclear 1D- and 2D-NMR study of the hydrolysis and condensation of bis-1,2-(triethoxysilyl)ethane. *J. Adhes. Sci. Technol.* **2004**, *18*, 765–778. [[CrossRef](#)]
61. Palanivel, V.M. Modified Silane Thin Films as an Alternative to Chromates for Corrosion Protection of AA2024-T3 Alloy. Ph.D. Thesis, University of Cincinnati, Cincinnati, OH, USA, 1957. Volume 9.
62. Figueira, R.B.; Fontinha, I.R.; Silva, C.J.R.; Pereira, E.V.; Yang, K.; van Ooij, W.J.; Seth, A.; Mugada, T.; Pan, G.; Schaefer, D.W.; et al. Hybrid sol-gel coatings: Smart and green materials for corrosion mitigation. *Prog. Org. Coat.* **2016**, *63*, 283–292. [[CrossRef](#)]
63. Trabelsi, W.; Dhoubi, L.; Triki, E.; Ferreira, M.G.S.; Montemor, M.F.; Cabral, A.M.; Duarte, R.G.; Montemor, M.F.; Zheludkevich, M.L.; Ferreira, M.G.S.; et al. Corrosion protection properties of organofunctional silanes—An overview. *Prog. Org. Coat.* **2005**, *48*, 639–664.
64. Mirabedini, S.M.; Thompson, G.E.; Moradian, S.; Scantlebury, J.D. Corrosion performance of powder coated aluminium using EIS. *Prog. Org. Coat.* **2003**, *46*, 112–120. [[CrossRef](#)]
65. Franquet, A.; Terryn, H.; Vereecken, J. IRSE study on effect of thermal curing on the chemistry and thickness of organosilane films coated on aluminium. *Appl. Surf. Sci.* **2003**, *211*, 259–269. [[CrossRef](#)]
66. Aïssa, B.; Therriault, D.; Haddad, E.; Jamroz, W. Self-healing materials systems: Overview of major approaches and recent developed technologies. *Adv. Mater. Sci. Eng.* **2012**, *2012*, 854203. [[CrossRef](#)]
67. Ji, W.G.; Hu, J.M.; Liu, L.; Zhang, J.Q.; Cao, C.N. Improving the corrosion performance of epoxy coatings by chemical modification with silane monomers. *Surf. Coat. Technol.* **2007**, *201*, 4789–4795. [[CrossRef](#)]
68. Kim, H.; Jang, J. Corrosion protection and adhesion promotion for polyimide/copper system using silane-modified polymeric materials. *Polymer* **2000**, *41*, 6553–6561. [[CrossRef](#)]
69. Chen, M.A.; Xie, X.; Zhang, X.M. Interactions of BTESPT silane and maleic anhydride grafted polypropylene with epoxy and application to improve adhesive durability between epoxy and aluminium sheet. *Prog. Org. Coat.* **2009**, *66*, 40–51. [[CrossRef](#)]

70. Cabral, A.; Duarte, R.G.; Montemor, M.F.; Zheludkevich, M.L.; Ferreira, M.G.S. Analytical characterisation and corrosion behaviour of bis-[triethoxysilylpropyl]tetrasulphide pre-treated AA2024-T3. *Corros. Sci.* **2005**, *47*, 869–881. [[CrossRef](#)]
71. Montoya, P.; Martins, C.R.; De Melo, H.G.; Aoki, I.V.; Jaramillo, F.; Calderón, J.A. Synthesis of polypyrrole-magnetite/silane coatings on steel and assessment of anticorrosive properties. *Electrochim. Acta* **2014**, *124*, 100–108. [[CrossRef](#)]
72. Nguyen Thi Le, H.; Bernard, M.C.; Garcia-Renaud, B.; Deslouis, C. Raman spectroscopy analysis of polypyrrole films as protective coatings on iron. *Synth. Met.* **2004**, *140*, 287–293. [[CrossRef](#)]
73. Herrasti, P.; Recio, F.J.; Ocón, P.; Fatás, E. Effect of the polymer layers and bilayers on the corrosion behaviour of mild steel: Comparison with polymers containing Zn microparticles. *Prog. Org. Coat.* **2005**, *54*, 285–291. [[CrossRef](#)]
74. Van Schaftinghen, T.; Deslouis, C.; Hubin, A.; Terry, H. Influence of the surface pre-treatment prior to the film synthesis, on the corrosion protection of iron with polypyrrole films. *Electrochim. Acta* **2006**, *51*, 1695–1703. [[CrossRef](#)]
75. Giacomelli, C.; Giacomelli, F.C.; Baptista, J.A.A.; Spinelli, A. The effect of oxalic acid on the corrosion of carbon steel. *Anti-Corros. Methods Mater.* **2004**, *51*, 105–111. [[CrossRef](#)]
76. Asan, A.; Kabasakaloglu, M. Electrochemical and corrosion behaviors of mild steel coated with polypyrrole. *Mater. Sci.* **2003**, *39*, 643–651. [[CrossRef](#)]
77. Rahman, S.U. Corrosion protection of steel by catalyzed polypyrrole films. *Surf. Coat. Technol.* **2011**, *205*, 3035–3042. [[CrossRef](#)]
78. Koene, L.; Hamer, W.J.; De Wit, J.H.W. Electrochemical behaviour of poly(pyrrole) coatings on steel. *J. Appl. Electrochem.* **2006**, *36*, 545–556. [[CrossRef](#)]
79. Grgur, B.N.; Krstajić, N.V.; Vojnović, M.V.; Lačnjevac, Č.; Gajić-Krstajić, L. The influence of polypyrrole films on the corrosion behavior of iron in acid sulfate solutions. *Prog. Org. Coat.* **1998**, *33*, 1–6. [[CrossRef](#)]
80. Grgur, B.N.; Živković, P.; Gvozdenović, M.M. Kinetics of the mild steel corrosion protection by polypyrrole-oxalate coating in sulfuric acid solution. *Prog. Org. Coat.* **2006**, *56*, 240–247. [[CrossRef](#)]
81. Ocón, P.; Cristobal, A.B.; Herrasti, P.; Fatas, E. Corrosion performance of conducting polymer coatings applied on mild steel. *Corros. Sci.* **2005**, *47*, 649–662. [[CrossRef](#)]
82. Roy, I. Synthesis, Surface Modification, Characterization, and Biomedical In Vitro Applications of Organically Modified Silica (ORMOSIL) Nanoparticles. In *Nanoparticles in Biology and Medicine: Methods and Protocols*; Soloviev, M., Ed.; Wiley-VCH Verlag GmbH & Co. KGaA: Weinheim, Germany, 2012; Volume 906, pp. 365–379, ISBN 9781617799532.
83. Kordas, G. Nanocontainers (CeO₂): Synthesis, Characterization, Properties, and Anti-corrosive Application. *ACS Symp. Ser.* **2021**, *1404*, 177–185.
84. Kordas, G. Nanocontainers for Enhanced Protection of HDG Steel Used in Concrete. *Materials* **2022**, *2*, 1–12.
85. Metroke, T.L.; Apblett, A. Effect of solvent dilution on corrosion protective properties of Ormosil coatings on 2024-T3 aluminum alloy. *Prog. Org. Coat.* **2004**, *51*, 36–46. [[CrossRef](#)]
86. Metroke, T.L.; Kachurina, O.; Knobbe, E.T. Spectroscopic and corrosion resistance characterization of GLYMO-TEOS Ormosil coatings for aluminum alloy corrosion inhibition. *Prog. Org. Coat.* **2002**, *44*, 295–305. [[CrossRef](#)]
87. Program, E.E.S.T.C. Non-Chromate Aluminum Pretreatments Phase II Interim Report. Available online: <http://www.iaindy.com/Documents/ncapii.pdf> (accessed on 18 April 2022).
88. Chung, Y.J.; Jeanjaquet, S.L.; Kendig, M.W. Normal Probability Function. US Patent 6,579,472 B2, 17 June 2003.
89. Fedrizzi, L.; Fürbeth, W.; Montemor, F. (Eds.) *Self-Healing Properties of New Surface Treatments*; NUMBER 58; European Federation of Corrosion, Institute of Materials, Minerals, and Mining; Wakefield, UK, 2011; Volume 47, ISBN 9781906540364.
90. Davenport, A.J.; Isaacs, H.S.; Kendig, M.W. XANES investigation of the role of cerium compounds as corrosion inhibitors for aluminum. *Corros. Sci.* **1991**, *32*, 653–663. [[CrossRef](#)]
91. Pourbaix, M. Atlas of Electrochemical Equilibria in Aqueous Solutions. *NACE Int.* **1974**, *307*, 194.
92. Hayes, S.A.; Yu, P.; O’Keefe, T.J.; O’Keefe, M.J.; Stoffer, J.O. The Phase Stability of Cerium Species in Aqueous Systems. *J. Electrochem. Soc.* **2002**, *149*, C623. [[CrossRef](#)]
93. Aldykiewicz, A.J.; Davenport, A.J.; Isaacs, H.S. Studies of the Formation of Cerium-Rich Protective Films Using X-Ray Absorption Near-Edge Spectroscopy and Rotating Disk Electrode Methods. *J. Electrochem. Soc.* **1996**, *143*, 147–154. [[CrossRef](#)]
94. Böhm, S.; Greef, R.; McMurray, H.N.; Powell, S.M.; Worsley, D.A. Kinetic and Mechanistic Studies of Rare Earth-Rich Protective Film Formation Using In Situ Ellipsometry. *J. Electrochem. Soc.* **2000**, *147*, 3286. [[CrossRef](#)]
95. Brusciotti, F.; Batan, A.; De Graeve, I.; Wenkin, M.; Biessemans, M.; Willem, R.; Reniers, F.; Pireaux, J.J.; Piens, M.; Vereecken, J.; et al. Characterization of thin water-based silane pre-treatments on aluminium with the incorporation of nano-dispersed CeO₂ particles. *Surf. Coat. Technol.* **2010**, *205*, 603–613. [[CrossRef](#)]
96. Cambon, J.B.; Esteban, J.; Ansart, F.; Bonino, J.P.; Turq, V.; Santagneli, S.H.; Santilli, C.V.; Pulcinelli, S.H. Effect of cerium on structure modifications of a hybrid sol-gel coating, its mechanical properties and anti-corrosion behavior. *Mater. Res. Bull.* **2012**, *47*, 3170–3176. [[CrossRef](#)]
97. Cabral, A.M.; Trabelsi, W.; Serra, R.; Montemor, M.F.; Zheludkevich, M.L.; Ferreira, M.G.S. The corrosion resistance of hot dip galvanised steel and AA2024-T3 pre-treated with bis-[triethoxysilylpropyl] tetrasulfide solutions doped with Ce(NO₃)₃. *Corros. Sci.* **2006**, *48*, 3740–3758. [[CrossRef](#)]
98. Montemor, M.F.; Ferreira, M.G.S. Cerium salt activated nanoparticles as fillers for silane films: Evaluation of the corrosion inhibition performance on galvanised steel substrates. *Electrochim. Acta* **2007**, *52*, 6976–6987. [[CrossRef](#)]

99. Farzi, G.; Davoodi, A.; Ahmadi, A.; Neisiany, R.E.; Anwer, M.K.; Aboudzadeh, M.A. Encapsulation of Cerium Nitrate within Poly(urea-formaldehyde) Microcapsules for the Development of Self-Healing Epoxy-Based Coating. *ACS Omega* **2021**, *6*, 31147–31153. [[CrossRef](#)]
100. Wang, H.; Akid, R. Encapsulated cerium nitrate inhibitors to provide high-performance anti-corrosion sol-gel coatings on mild steel. *Corros. Sci.* **2008**, *50*, 1142–1148. [[CrossRef](#)]
101. Trabelsi, W.; Cecilio, P.; Ferreira, M.G.S.; Montemor, M.F. Electrochemical assessment of the self-healing properties of Ce-doped silane solutions for the pre-treatment of galvanised steel substrates. *Prog. Org. Coat.* **2005**, *54*, 276–284. [[CrossRef](#)]
102. Pepe, A.; Aparicio, M.; Durán, A.; Ceré, S. Cerium hybrid silica coatings on stainless steel AISI 304 substrate. *J. Sol-Gel Sci. Technol.* **2006**, *39*, 131–138. [[CrossRef](#)]
103. Pepe, A.; Aparicio, M.; Ceré, S.; Durán, A. Preparation and characterization of cerium doped silica sol-gel coatings on glass and aluminum substrates. *J. Non. Cryst. Solids* **2004**, *348*, 162–171. [[CrossRef](#)]
104. Trabelsi, W.; Triki, E.; Dhoubi, L.; Ferreira, M.G.S.; Zheludkevich, M.L.; Montemor, M.F. The use of pre-treatments based on doped silane solutions for improved corrosion resistance of galvanised steel substrates. *Surf. Coat. Technol.* **2006**, *200*, 4240–4250. [[CrossRef](#)]
105. Voevodin, N.N.; Grebasch, N.T.; Soto, W.S.; Arnold, F.E.; Donley, M.S. Potentiodynamic evaluation of sol-gel coatings with inorganic inhibitors. *Surf. Coat. Technol.* **2001**, *140*, 24–28. [[CrossRef](#)]
106. Morozova, M.; Kluson, P.; Krysa, J.; Zlamal, M.; Solcova, O.; Kment, S.; Steck, T. Role of the template molecular structure on the photo-electrochemical functionality of the sol-gel titania thin films. *J. Sol-Gel Sci. Technol.* **2009**, *52*, 398–407. [[CrossRef](#)]
107. Schem, M.; Schmidt, T.; Gerwann, J.; Wittmar, M.; Veith, M.; Thompson, G.E.; Molchan, I.S.; Hashimoto, T.; Skeldon, P.; Phani, A.R.; et al. CeO₂-filled sol-gel coatings for corrosion protection of AA2024-T3 aluminium alloy. *Corros. Sci.* **2009**, *51*, 2304–2315. [[CrossRef](#)]
108. Zhu, D.; Van Ooij, W.J. Corrosion protection of metals by water-based silane mixtures of bis-[trimethoxysilylpropyl]amine and vinyltriacetoxysilane. *Prog. Org. Coat.* **2004**, *49*, 42–53. [[CrossRef](#)]
109. Owczarek, E. Methods of modifying anticorrosive protective properties of silane films. *Acta Phys. Pol. A* **2019**, *135*, 147–152. [[CrossRef](#)]
110. Yu, Z.; Hu, J.; Meng, H. A Review of Recent Developments in Coating Systems for Hot-Dip Galvanized Steel. *Front. Mater.* **2020**, *7*, 74. [[CrossRef](#)]
111. Kozaderov, O.; Shikhaliev, K.; Prabhakar, C.; Tripathi, A.; Shevtsov, D.; Kruzhilin, A.; Komarova, E.; Potapov, A.; Zartsyn, I.; Kuznetsov, Y. Corrosion of α -Brass in Solutions Containing Chloride Ions and 3-Mercaptoalkyl-5-amino-1,2,4-triazoles. *Appl. Sci.* **2019**, *9*, 2821. [[CrossRef](#)]
112. Özcan, M.; Dehri, I.; Erbil, M. Organic sulphur-containing compounds as corrosion inhibitors for mild steel in acidic media: Correlation between inhibition efficiency and chemical structure. *Appl. Surf. Sci.* **2004**, *236*, 155–164. [[CrossRef](#)]
113. Marconato, J.C.; Bulhões, L.O.; Temperin, M.L. A spectroelectrochemical study of the inhibition of the electrode process on copper by 2-mercaptobenzothiazole in ethanolic solutions. *Electrochim. Acta* **1997**, *43*, 771–780. [[CrossRef](#)]
114. Ebenso, E.E.; Isabirye, D.A.; Eddy, N.O. Adsorption and quantum chemical studies on the inhibition potentials of some thiosemicarbazides for the corrosion of mild steel in acidic medium. *Int. J. Mol. Sci.* **2010**, *11*, 2473–2498. [[CrossRef](#)]
115. Balaskas, A.C.; Curioni, M.; Thompson, G.E. Corrosion protection mechanism of 2-mercaptobenzothiazole and its potential synergistic effect with cerium ions for treatment of AA 2024-T3. *J. Electroanal. Chem.* **2020**, *863*, 114081. [[CrossRef](#)]
116. Lamaka, S.V.; Zheludkevich, M.L.; Yasakau, K.A.; Montemor, M.F.; Ferreira, M.G.S.S. High effective organic corrosion inhibitors for 2024 aluminium alloy. *Electrochim. Acta* **2007**, *52*, 7231–7247. [[CrossRef](#)]
117. Tan, B.; Zhang, S.; Cao, X.; Fu, A.; Guo, L.; Marzouki, R.; Li, W. Insight into the anti-corrosion performance of two food flavors as eco-friendly and ultra-high performance inhibitors for copper in sulfuric acid medium. *J. Colloid Interface Sci.* **2022**, *609*, 838–851. [[CrossRef](#)] [[PubMed](#)]
118. Tan, B.; Lan, W.; Zhang, S.; Deng, H.; Qiang, Y.; Fu, A.; Ran, Y.; Xiong, J.; Marzouki, R.; Li, W. Passiflora edulia Sims leaves Extract as renewable and degradable inhibitor for copper in sulfuric acid solution. *Colloids Surf. A Physicochem. Eng. Asp.* **2022**, *645*, 128892. [[CrossRef](#)]
119. Balaskas, A.; Curioni, M.; Thompson, G. Effectiveness of 2-mercaptobenzothiazole, 8-hydroxyquinoline and benzotriazol as corrosion inhibitors on AA 2024-T3 assessed by electrochemical methods. *Surf. Interface Anal.* **2015**, *47*, 1029–1039. [[CrossRef](#)]
120. Curioni, M.; Balaskas, A.C.; Thompson, G.E. An alternative to the use of a zero resistance ammeter for electrochemical noise measurement: Theoretical analysis, experimental validation and evaluation of electrode asymmetry. *Corros. Sci.* **2013**, *77*, 281–291. [[CrossRef](#)]
121. Balaskas, A.C.; Curioni, M.; Thompson, G.E. Evaluation of Inhibitor Performance by Electrochemical Methods: Comparative Study of Nitrate Salts on AA 2024-T3. *J. Electrochem. Soc.* **2014**, *161*, C389–C394. [[CrossRef](#)]
122. Li, S.M.; Zhang, H.R.; Liu, J.H. Corrosion behavior of aluminum alloy 2024-T3 by 8-hydroxy-quinoline and its derivative in 3.5% chloride solution. *Trans. Nonferrous Met. Soc. China* **2007**, *17*, 318–325. [[CrossRef](#)]
123. Wang, A.Q.; Golden, T.D. Anodic Electrodeposition of Cerium Oxide Thin Films. *J. Electrochem. Soc.* **2003**, *150*, C616. [[CrossRef](#)]
124. Kartsonakis, I.; Daniilidis, I.; Kordas, G. Encapsulation of the corrosion inhibitor 8-hydroxyquinoline into ceria nanocontainers. *J. Sol-Gel Sci. Technol.* **2008**, *48*, 24–31. [[CrossRef](#)]

125. Liu, L.; Hu, J.M.; Zhang, J.Q.; Cao, C.N. Improving the formation and protective properties of silane films by the combined use of electrodeposition and nanoparticles incorporation. *Electrochim. Acta* **2006**, *52*, 538–545. [[CrossRef](#)]
126. Phanasgaonkar, A.; Raja, V.S. Influence of curing temperature, silica nanoparticles- and cerium on surface morphology and corrosion behaviour of hybrid silane coatings on mild steel. *Surf. Coat. Technol.* **2009**, *203*, 2260–2271. [[CrossRef](#)]
127. Chen, Y.; Jin, L.; Xie, Y. Sol-Gel Processing of Organic-Inorganic Nanocomposite Protective Coatings. *J. Sol-Gel Sci. Technol.* **1998**, *13*, 735–738. [[CrossRef](#)]
128. Wu, L.; Yang, H.; Wang, H.; Lu, J. Electrosynthesis of cyclic carbonates from CO₂ and epoxides on a reusable copper nanoparticle cathode. *RSC Adv.* **2015**, *5*, 23189–23192. [[CrossRef](#)]
129. Asadi, N.; Naderi, R.; Saremi, M.; Arman, S.Y.; Fedel, M.; Deflorian, F. Study of corrosion protection of mild steel by eco-friendly silane sol-gel coating. *J. Sol-Gel Sci. Technol.* **2014**, *70*, 329–338. [[CrossRef](#)]
130. Ramezanzadeh, B.; Ahmadi, A.; Mahdavian, M. Enhancement of the corrosion protection performance and cathodic delamination resistance of epoxy coating through treatment of steel substrate by a novel nanometric sol-gel based silane composite film filled with functionalized graphene oxide nanosheets. *Corros. Sci.* **2016**, *109*, 182–205. [[CrossRef](#)]
131. Zheludkevich, M.L.; Serra, R.; Montemor, M.F.; Yasakau, K.A.; Salvado, I.M.M.; Ferreira, M.G.S. Nanostructured sol-gel coatings doped with cerium nitrate as pre-treatments for AA2024-T3 Corrosion protection performance. *Electrochim. Acta* **2005**, *51*, 208–217. [[CrossRef](#)]
132. Cant, N.E.; Critchley, K.; Zhang, H.L.; Evans, S.D. Surface functionalisation for the self-assembly of nanoparticle/polymer multilayer films. *Thin Solid Films* **2003**, *426*, 31–39. [[CrossRef](#)]
133. Palanivel, V.; Zhu, D.; Van Ooij, W.J. Nanoparticle-filled silane films as chromate replacements for aluminum alloys. *Prog. Org. Coat.* **2003**, *47*, 384–392. [[CrossRef](#)]
134. Carraro, M.; Gross, S. Hybrid materials based on the embedding of organically modified transition metal oxoclusters or polyoxometalates into polymers for functional applications: A review. *Materials* **2014**, *7*, 3956–3989. [[CrossRef](#)]
135. Zheludkevich, M.L.; Serra, R.; Montemor, M.F.; Ferreira, M.G.S. Oxide nanoparticle reservoirs for storage and prolonged release of the corrosion inhibitors. *Electrochem. Commun.* **2005**, *7*, 836–840. [[CrossRef](#)]
136. Susac, D.; Leung, C.W.; Sun, X.; Wong, K.C.; Mitchell, K.A.R. Comparison of a chromic acid and a BTSE final rinse applied to phosphated 2024-T3 aluminum alloy. *Surf. Coat. Technol.* **2004**, *187*, 216–224. [[CrossRef](#)]
137. Biedunkiewicz, A.; Gordon, N.; Straszko, J.; Tamir, S. Kinetics of thermal oxidation of titanium carbide and its carbon nanocomposites in dry air atmosphere. *J. Therm. Anal. Calorim.* **2007**, *88*, 717–722. [[CrossRef](#)]
138. Wittmar, A.; Wittmar, M.; Caparrotti, H.; Veith, M. The influence of the inhibitor particle sizes to the corrosion properties of hybrid sol-gel coatings. *J. Sol-Gel Sci. Technol.* **2011**, *59*, 621–628. [[CrossRef](#)]
139. Trenado, C.; Wittmar, M.; Veith, M.; Rosero-Navarro, N.C.; Aparicio, M.; Durn, A.; Castro, Y.; Strauss, D.J. Multiscale numerical modeling of Ce³⁺-inhibitor release from novel corrosion protection coatings. *Model. Simul. Mater. Sci. Eng.* **2011**, *19*, 025009. [[CrossRef](#)]
140. Rosero-Navarro, N.C.; Pausa, L.; Andreatta, F.; Castro, Y.; Durán, A.; Aparicio, M.; Fedrizzi, L. Optimization of hybrid sol-gel coatings by combination of layers with complementary properties for corrosion protection of AA2024. *Prog. Org. Coat.* **2010**, *69*, 167–174. [[CrossRef](#)]
141. Palermo, E.F.; Lee, D.K.; Ramamoorthy, A.; Kuroda, K. Role of cationic group structure in membrane binding and disruption by amphiphilic copolymers. *J. Phys. Chem. B* **2011**, *115*, 366–375. [[CrossRef](#)]
142. Gite, V.V.; Tatiya, P.D.; Marathe, R.J.; Mahulikar, P.P.; Hundiwale, D.G. Microencapsulation of quinoline as a corrosion inhibitor in polyurea microcapsules for application in anticorrosive PU coatings. *Prog. Org. Coat.* **2015**, *83*, 11–18. [[CrossRef](#)]
143. Kartsonakis, I.A.; Balaskas, A.C.; Kordas, G.C. Influence of TiO₂ nanocontainers on hybrid organic-inorganic coatings for corrosion protection of magnesium alloy. *Int. J. Struct. Integr.* **2013**, *4*, 127–142. [[CrossRef](#)]
144. Szabó, T.; Molnár-Nagy, L.; Bognár, J.; Nyikos, L.; Telegdi, J. Self-healing microcapsules and slow release microspheres in paints. *Prog. Org. Coat.* **2011**, *72*, 52–57. [[CrossRef](#)]
145. Samadzadeh, M.; Boura, S.H.; Peikari, M.; Kasiriha, S.M.; Ashrafi, A. A review on self-healing coatings based on micro/nanocapsules. *Prog. Org. Coat.* **2010**, *68*, 159–164. [[CrossRef](#)]
146. Thanawala, K.; Mutneja, N.; Khanna, A.S.; Singh Raman, R.K. Development of self-healing coatings based on linseed oil as autonomous repairing agent for corrosion resistance. *Materials* **2014**, *7*, 7324–7338. [[CrossRef](#)]
147. Kartsonakis, I.A.; Kontogiani, P.; Pappas, G.S.; Kordas, G. Photocatalytic action of cerium molybdate and iron-titanium oxide hollow nanospheres on *Escherichia coli*. *J. Nanoparticle Res.* **2013**, *15*, 1759. [[CrossRef](#)]
148. Kartsonakis, I.A.; Koumoulos, E.P.; Charitidis, C.A.; Kordas, G. Hybrid organic-inorganic coatings including nanocontainers for corrosion protection of magnesium alloy ZK30 Nanostructured Materials 2012. Special Issue Editors: Juan Manuel Rojo, Vasileios Koutsos. *J. Nanoparticle Res.* **2013**, *15*, 1871. [[CrossRef](#)]
149. Kordas, G.C.; Balaskas, A.C.; Kartsonakis, I.A.; Efthimiadou, E.K. A Raman study of 8-Hydroxyquinoline release from loaded TiO₂ nanocontainer. *Int. J. Struct. Integr.* **2013**, *4*, 121–126. [[CrossRef](#)]
150. Parameswaranpillai, J.; Salim, N.V.; Pulikkalparambil, H.; Rangappa, S.M.; Siengchin, I.; Habel, S. *Micro- and Nano-containers for Smart Applications*; Springer Nature Singapore Pte Ltd.: Singapore, 2022; ISBN 9789811681455.
151. Rule, J.D.; Sottos, N.R.; White, S.R. Effect of microcapsule size on the performance of self-healing polymers. *Polymer* **2007**, *48*, 3520–3529. [[CrossRef](#)]

152. Borisova, D.; Möhwald, H.; Shchukin, D.G. Influence of embedded nanocontainers on the efficiency of active anticorrosive coatings for aluminum alloys part II: Influence of nanocontainer position. *ACS Appl. Mater. Interfaces* **2013**, *5*, 80–87. [[CrossRef](#)] [[PubMed](#)]
153. Kartsonakis, I.A.; Athanasopoulou, E.; Snihirova, D.; Martins, B.; Koklioti, M.A.; Montemor, M.F.; Kordas, G.; Charitidis, C.A. Multifunctional epoxy coatings combining a mixture of traps and inhibitor loaded nanocontainers for corrosion protection of AA2024-T3. *Corros. Sci.* **2014**, *85*, 147–159. [[CrossRef](#)]
154. Krzak, M.; Tabor, Z.; Nowak, P.; Warszyński, P.; Karatzas, A.; Kartsonakis, I.A.; Kordas, G.C.; Warszy, P.; Karatzas, A.; Kartsonakis, I.A.; et al. Water diffusion in polymer coatings containing water-trapping particles. Part 2. Experimental verification of the mathematical model. *Prog. Org. Coat.* **2012**, *75*, 207–214. [[CrossRef](#)]
155. Buchheit, R.G.; Guan, H.; Mahajanam, S.; Wong, F. Active corrosion protection and corrosion sensing in chromate-free organic coatings. *Prog. Org. Coat.* **2003**, *47*, 174–182. [[CrossRef](#)]
156. Zheludkevich, M.L.; Poznyak, S.K.; Rodrigues, L.M.; Raps, D.; Hack, T.; Dick, L.F.; Nunes, T.; Ferreira, M.G.S.S. Active protection coatings with layered double hydroxide nanocontainers of corrosion inhibitor. *Corros. Sci.* **2010**, *52*, 602–611. [[CrossRef](#)]
157. Tedim, J.; Kuznetsova, A.; Salak, A.N.; Montemor, F.; Snihirova, D.; Pilz, M.; Zheludkevich, M.L.; Ferreira, M.G.S. Zn-Al layered double hydroxides as chloride nanotraps in active protective coatings. *Corros. Sci.* **2012**, *55*, 1–4. [[CrossRef](#)]
158. Montemor, M.F.; Snihirova, D.V.; Taryba, M.G.; Lamaka, S.V.; Kartsonakis, I.A.; Balaskas, A.C.; Kordas, G.C.; Tedim, J.; Kuznetsova, A.; Zheludkevich, M.L.; et al. Evaluation of self-healing ability in protective coatings modified with combinations of layered double hydroxides and cerium molybdate nanocontainers filled with corrosion inhibitors. *Electrochim. Acta* **2012**, *60*, 31–40. [[CrossRef](#)]
159. Shchukin, B.D.G.; Zheludkevich, M.; Yasakau, K.; Lamaka, S.; Ferreira, M.G.S.; Möhwald, H. Layer-by-Layer Assembled Nanocontainers for Self-Healing Corrosion Protection. *Adv. Mater.* **2006**, *18*, 1672–1678. [[CrossRef](#)]
160. Sonawane, S.H.; Bhanvase, B.A.; Jamali, A.A.; Dubey, S.K.; Kale, S.S.; Pinjari, D.V.; Kulkarni, R.D.; Gogate, P.R.; Pandit, A.B. Improved active anticorrosion coatings using layer-by-layer assembled ZnO nanocontainers with benzotriazole. *Chem. Eng. J.* **2012**, *189*, 464–472. [[CrossRef](#)]
161. Bhanvase, B.A.; Patel, M.A.; Sonawane, S.H. Kinetic properties of layer-by-layer assembled cerium zinc molybdate nanocontainers during corrosion inhibition. *Corros. Sci.* **2014**, *88*, 170–177. [[CrossRef](#)]
162. Balaskas, A.C.; Kartsonakis, I.; Bilalis, P.; Karatzas, A.; Kordas, G. Epoxy Coatings Containing Nanocontainers Loaded with Corrosion Inhibitors for Corrosion Protection of AA 2024-T3. *ECS Meet. Abstr.* **2011**, MA2011-02, 1656. [[CrossRef](#)]
163. Balaskas, A.C.; Hashimoto, T.; Curioni, M.; Thompson, G.E. Two-shell structured PMAA@CeO₂ nanocontainers loaded with 2-mercaptobenzothiazole for corrosion protection of damaged epoxy coated AA 2024-T3. *Nanoscale* **2017**, *9*, 5499–5508. [[CrossRef](#)]
164. Chenan, A.; Ramya, S.; George, R.P.; Kamachi Mudali, U. Hollow mesoporous zirconia nanocontainers for storing and controlled releasing of corrosion inhibitors. *Ceram. Int.* **2014**, *40*, 10457–10463. [[CrossRef](#)]
165. Chenan, A.; Ramya, S.; George, R.P.; Mudali, U.K. 2-mercaptobenzothiazole-loaded hollow mesoporous silica-based hybrid coatings for corrosion protection of modified 9Cr-1Mo ferritic steel. *Corrosion* **2014**, *70*, 496–511. [[CrossRef](#)]
166. Chen, T.; Chen, R.; Jin, Z.; Liu, J. Engineering hollow mesoporous silica nanocontainers with molecular switches for continuous self-healing anticorrosion coating. *J. Mater. Chem. A* **2015**, *3*, 9510–9516. [[CrossRef](#)]
167. Qian, B.; Michailidis, M.; Bilton, M.; Hobson, T.; Zheng, Z.; Shchukin, D. Tannic complexes coated nanocontainers for controlled release of corrosion inhibitors in self-healing coatings. *Electrochim. Acta* **2019**, *297*, 1035–1041. [[CrossRef](#)]
168. Manasa, S.; Jyothirmayi, A.; Siva, T.; Sathiyarayanan, S.; Gobi, K.V.; Subasri, R. Effect of inhibitor loading into nanocontainer additives of self-healing corrosion protection coatings on aluminum alloy A356.0. *J. Alloys Compd.* **2017**, *726*, 969–977. [[CrossRef](#)]
169. Manasa, S.; Siva, T.; Sathiyarayanan, S.; Gobi, K.V.; Subasri, R. Montmorillonite nanoclay-based self-healing coatings on AA 2024-T4. *J. Coat. Technol. Res.* **2018**, *15*, 721–735. [[CrossRef](#)]
170. He, Y.; Zhang, C.; Wu, F.; Xu, Z. Fabrication study of a new anticorrosion coating based on supramolecular nanocontainer. *Synth. Met.* **2016**, *212*, 186–194. [[CrossRef](#)]
171. Shchukin, D.G.; Lamaka, S.V.; Yasakau, K.A.; Zheludkevich, M.L.; Ferreira, M.G.S.; Möhwald, H. Active anticorrosion coatings with halloysite nanocontainers. *J. Phys. Chem. C* **2008**, *112*, 958–964. [[CrossRef](#)]
172. Yabuki, A.; Shiraiwa, T.; Fathona, I.W. pH-controlled self-healing polymer coatings with cellulose nanofibers providing an effective release of corrosion inhibitor. *Corros. Sci.* **2016**, *103*, 117–123. [[CrossRef](#)]
173. Sauvaut-Moynot, V.; Gonzalez, S.; Kittel, J.; Leal, D.A.; Riegel-Vidotti, I.C.; Ferreira, M.G.S.; Marino, C.E.B.; Lv, L.P.; Zhao, Y.; Vilbrandt, N.; et al. Engineering hollow mesoporous silica nanocontainers with molecular switches for continuous self-healing anticorrosion coating. *Corros. Sci.* **2018**, *3*, 5499–5508.
174. Song, Y.; Jo, Y.; Lim, Y.; Cho, S.; Yu, H.; Ryu, B.; Lee, S.; Chung, C. Sunlight-Induced Self-Healing of a Microcapsule-Type Protective Coating. *Appl. Mater. Interfaces* **2013**, *5*, 378–384. [[CrossRef](#)]
175. Zhao, Y.; Berger, R.; Landfester, K.; Crespy, D. Double Redox-Responsive Release of Encoded and Encapsulated Molecules from Patchy Nanocapsules. *Small* **2015**, *11*, 2995–2999. [[CrossRef](#)]
176. Saji, V.S. Supramolecular concepts and approaches in corrosion and biofouling prevention. *Corros. Rev.* **2019**, *37*, 187–230. [[CrossRef](#)]

177. Ding, C.; Xu, J.; Tong, L.; Gong, G.; Jiang, W.; Fu, J. Design and Fabrication of a Novel Stimulus-Feedback Anticorrosion Coating Featured by Rapid Self-healing Functionality for Protection of Magnesium Alloy. *ACS Appl. Mater. Interfaces 'HVLJQ* **2017**, *9*, 21034–21047. [[CrossRef](#)]
178. Wheat, H.G.; Liu, G. Coatings for Early Corrosion Detection. *ECS Meet. Abstr.* **2010**, *MA2010-01*, 903. [[CrossRef](#)]
179. Frankel, G.S. Corrosion-sensing behavior of an acrylic-based coating system. *Corrosion* **1999**, *55*, 957–967.
180. Sibi, M.P.; Zong, Z. Determination of corrosion on aluminum alloy under protective coatings using fluorescent probes. *Prog. Org. Coat.* **2003**, *47*, 8–15. [[CrossRef](#)]
181. Augustyniak, A.; Tsavalas, J.; Ming, W. Early detection of steel corrosion via “turn-On” fluorescence in smart epoxy coatings. *ACS Appl. Mater. Interfaces* **2009**, *1*, 2618–2623. [[CrossRef](#)] [[PubMed](#)]
182. Calle, M.; Li, W.; Buhrow, J.W.; Johnsey, M.N.; Jolley, S.T.; Benjamin, P.; Zhang, X.; Fitzpatrick, L.; Gillis, M.; Blanton, M.; et al. Environmentally Friendly Coating Technology for Autonomous Corrosion Control. In Proceedings of the 43rd Annual Waterborne Symposium, New Orleans, LA, USA, 31 January–5 February 2016; Volume 32899.
183. Liu, G.; Wheat, H.G. Use of a Fluorescent Indicator in Monitoring Underlying Corrosion on Coated Aluminum 2024-T4. *J. Electrochem. Soc.* **2009**, *156*, C160. [[CrossRef](#)]
184. Mata, D.; Scharnagl, N.; Lamaka, S.V.; Malheiro, E.; Maia, F.; Zheludkevich, M.L. Validating the early corrosion sensing functionality in poly (ether imide) coatings for enhanced protection of magnesium alloy AZ31. *Corros. Sci.* **2018**, *140*, 307–320. [[CrossRef](#)]
185. Maia, F.; Tedim, J.; Bastos, A.C.; Ferreira, M.G.S.; Zheludkevich, M.L. Nanocontainer-based corrosion sensing coating. *Nanotechnology* **2013**, *24*, 415502. [[CrossRef](#)]
186. Wankhede, R.G.; Morey, S.; Khanna, A.S.; Birbilis, N. Development of water-repellent organic-inorganic hybrid sol-gel coatings on aluminum using short chain perfluoro polymer emulsion. *Appl. Surf. Sci.* **2013**, *283*, 1051–1059. [[CrossRef](#)]
187. Thermo Fisher Scientific ASTM B117. *Mater. Saf. Data Sheet* **2012**, *4*, 8–10.
188. Kordas, G. CuO (Bromosphaerol) and CeMo (8 Hydroxyquinoline) microcontainers incorporated into commercial marine paints. *J. Am. Ceram. Soc.* **2020**, *103*, 2340–2350. [[CrossRef](#)]
189. Kordas, G. Novel Antifouling and Self-Healing Eco-Friendly Coatings for Marine Applications Enhancing the Performance of Commercial Marine Paints. In *Engineering Failure Analysis*; IntechOpen: London, UK, 2020; pp. 1–9.
190. Kordas, G. Nanotechnology to improve the biofouling and corrosion performance of marine paints: From lab experiments to real tests in sea. *Int. J. Phys. Res. Appl.* **2019**, *2*, 33–37. [[CrossRef](#)]
191. Kordas, G. Nanocontainers-Based Anti-Biofouling Coatings—A Pilot Study. In *Supramolecular Chemistry in Corrosion and Biofouling Protection*; Saji, V.S., Ed.; CRC Press: London, UK, 2021; pp. 383–392, ISBN 9781003169130.
192. Thomas, S.; Surendran, A. (Eds.) *Self-Healing Polymer-Based Systems*; Elsevier: Amsterdam, The Netherlands, 2020; ISBN 9780128184509.